Spring 1986

Laser Pump and Probe Excited State Absorption Measurements

Shawpin Jong
Old Dominion University

LASER PUMP AND PROBE

EXCITED STATE ABSORPTION MEASUREMENTS

by

Shawpin Jong
B.S. June 1980, Fu Jen Catholic University

A Thesis Submitted to the Faculty of
Old Dominion University in Partial Fulfillment of the
Requirements for the Degree of

MASTER OF ENGINEERING

ELECTRICAL ENGINEERING

OLD DOMINION UNIVERSITY

April 1986

Approved by:

Amin N. Dharamsi (Director)

Karl H. Schoenbach

Joseph L. Hibey

LASER PUMP AND PROBE

EXCITED STATE ABSORPTION MEASUREMENTS

by

Shawpin Jong
B.S. June 1980, Fu Jen Catholic University

A Thesis Submitted to the Faculty of
Old Dominion University in Partial Fulfillment of the
Requirements for the Degree of

MASTER OF ENGINEERING

ELECTRICAL ENGINEERING

OLD DOMINION UNIVERSITY

April 1986

ABSTRACT

LASER PUMP AND PROBE
EXCITED STATE ABSORPTION MEASUREMENTS

Shawpin Jong
Old Dominion University, 1986
Director: Dr. Amin N. Dharamsi

A pump and probe technique was used to investigate triplet-triplet excited state absorption in solutions of the scintillators 2,5 diphenyloxazole (PPO) and 2,1 naphthyl,5 phenylzole (α-NPO) in several solvents.

KrF excimer radiation (248 nm) was used to pump the samples under investigation as well as a tunable dye laser which was used as the probe. Time-resolution was obtained by changing the optical path difference between the pump and probe beams.

Transient excited state absorption was measured in a wide spectral region between 330 nm and 600 nm, showing a peak at 400 nm for PPO solutions, and two peaks at 390 nm and 455nm respectively for α-NPO solutions. After the excimer pump excited the sample, the absorption peaked approximately 110 ns and 60 ns for PPO and α-NPO respectively. Fluorescence from the $S_1 \rightarrow S_0$ band was monitored simultaneously.

The effect of varying concentrations (in the range between 10^{-1} M and 10^{-7} M) was investigated. Both the fluorescence and excited state absorption displayed a concentration quenching effect for PPO in cyclohexane and 1,4 dioxane, and for α-NPO in 1,4 dioxane. The maxima occurred at approximately 10^{-3} M. No such self-quenching was observed for toluene solutions.

A numerical analysis of the relevant rate equations for the molecular excitations and deexcitation processes was performed. This analysis yielded some rate constants that have not been measured previously. For example: K_{isc}, the intersystem crossing rate for PPO was found to be 2.9×10^{6} sec^{-1} and that for α-NPO to be 3.3×10^{6} sec^{-1}; K_e, the excimer formation rate for α-NPO was measured as 7.5×10^{-12} $cm^3 - sec^{-1}$; $K_{t'}$, the quenching by O_2 of PPO triplets is 1.6×10^{5} sec^{-1} while for α-NPO it is 2.5×10^{6} sec^{-1}. K_{tt}, the triplet-triplet self-quenching rate for PPO is 3.2×10^{-12} $cm^3 - sec^{-1}$ and for α-NPO it is 6.8×10^{-11} $cm^3 - sec^{-1}$.

ACKNOWLEDGEMENTS

I would like to express my deepest appreciation to Dr. Amin N. Dharamsi for his guidance, patience, and support during the research and preparation of this thisis. Without his advice this work could never have been accomplished.

I also wish to thank my committee members, Dr. Joseph L. Hibey and Dr. Karl H. Schoenbach for their help and constructive criticisms. The assistance of Dr. John V. Shebalin and Dr. A. B. Hassam (U. of Maryland) is also gratefully acknowledged.

Special thanks go to Mr. Wen-Long Wu for his help in preparing this work.

Finally, my wife Haw-Lin made repeated sacrifices so I could complete this project. She was a constant source of praise and encouragement and never gave up on me. I only hope the dedication symbolizes the importance of her, and all she does, to my life.

TABLE OF CONTENTS

PAGE

LIST OF TABLES

LIST OF FIGURES

LIST OF FIGURES(Continued)

LIST OF FIGURES(Continued)

Chapter I

INTRODUCTION

This chapter gives an outline of the thesis and summarizes the results obtained. We used a pump and probe technique to investigate excited state absorption in both solution and vapor phase of some organic molecules. Triplet-Triplet excited state absorption was found for scintillator molecules such as 2,5 diphenyloxaazole (PPO) and 2,1 naphthyl,5 phenylzole (α-NPO) in solution in various solvents. The results of this work have also been described in reference [1].

KrF excimer laser radiation (248 nm) was used to pump the samples under investigation as well as a tunable dye laser which was used as the probe. In this way, jitter-free time-resolution was obtained by changing the optical path difference between the pump and probe beams.

Transient excited state absorption was measured in a wide spectral region between 330 nm and 600 nm, for PPO solutions, showing a peak at 400 nm. α-NPC solutions exhibited two peaks, at 390 nm and 455 nm respectively. This absorption was found to be due to triplet states. Time-resolved experiments showed that these triplets peaked

at 60 ns (α-NPO) and 110 ns (PPO) after the excimer pump. Fluorescence from the $S_1 \rightarrow S_o$ band was monitored simultaneously.

All measurements were carried out in solutions. Various solvents were used. The effect of varying concentration (10^{-1} M to 10^{-7} M) was investigated. Both the fluorescence and excited state absorption displayed a concentration quenching effect. The maxima occurred for concentrations between 10^{-3} M and 10^{-4} M. No such self-quenching was observed for both scintillators in toluene solutions. In every case, however, the fluorescence and excited state absorption measurements showed good correlation, as would be expected, since the T_1 state is formed directly from the S_1 states by intersystem crossing. These results are explained in terms of the quenching of S_1 states (and consequently a depletion of T_1 states) via excimer formation at higher concentration in the non-aromatic solvents.

The effect of dissolved oxygen on these measurements was investigated by performing experiments in air-equilibrated, deoxygenated and oxygen saturated solutions. Preliminary experiments with a 351 nm XeF pump were also conducted and yielded results which were essentially similar to those obtained with the 248 nm pump.

There is substantial overlap between the excited state triplet-triplet absorption spectra we measured and the

fluorescence band of both PPO and α-NPO [2], which is not very surprising since it is well-known that such overlap is one of the major reasons why a build up of triplet states is so detrimental to the performance of dye lasers [3].

Another motivation for studying excited state triplet-triplet absorption, to be described in this thesis is the importance of triplet states in many photophysical and photochemical processes [4,8,9]. We are particularly interested in assessing the feasibility of using triplet-triplet exchange for pumping certain types of lasers [5-7]. Further, an understanding of triplet state kinetics is necessary in the theory and practice of scintillation counting, since it is the accumulation of triplets that gives rise to the delayed scintillation component [10].

The second part of this investigation is to set up a theoretical model by deriving the rate equations for the singlet and triplet states.

A numerical analysis on a VAX11/780 computer was performed. This analysis agrees very well with the experimental results. By this method, we were able to measure some rate constants that have not been obtained previously. For example, the intersystem-crossing rate (K_{isc}), the rate of triplet quenching by O_2 (K_t), the rate of excimer formation (K_e), and the rate for triplet-triplet self-quenching (K_{tt}).

Chapter II gives some background to the work we performed. This includes a brief description of previous work, the motivation for our work, and some other relevant theoretical background. This is followed by a detailed description of the experimental apparatus in chapter III. Chapter IV describes the experimental results obtained. Chapter V develops the relevant rate equations describing the molecular processes occurring in the sample solutions. A comparison of the results obtained by numerical analysis of these rate equations with the experimental ones is also given. Finally, conclusions and suggestions for further investigation are presented in chapter VI.

Chapter II

BACKGROUND

THE ABSORPTION MECHANISM

Ultraviolet spectroscopy has its beginnings in the mid-19th century when Lambert [13] found that absorption of monochromatic light is exponentially related to the thickness of the absorbing material:

$$I = I_o \exp(- U d) \qquad (II-1)$$

where I_o is the incident light intensity,

I the emerging light intensity,

U a constant, characteristic of the material and wavelength of the light being absorbed,

and d the thickness of the layer of absorbing material.

Shortly after Beer found that in solutions, the constant U is directly related to the concentration of the material absorbing the light. Thus,

$$\log(I_o/I) = \varepsilon [M] d \; . \qquad (II-2)$$

Where ε is the molar extinction coefficient of the molecule at one particular wavelength. Generally,

ultraviolet and visible spectra are reported with the molar extinction coefficient, ε, measured at the wavelength of maximum absorption, λ_{max}.

The radiant energy is transferred to the molecule by a mechanism involving excitations of some higher molecular energy state. Figure 2-1 is a simple diagram which shows the energy transitions that may be involved when a molecule is so pumped.

The molecule is excited to one of the excited singlet states (S_1 or S_2), and through a series of radiationless transitions, called internal conversions, it drops back to the excited singlet state of lowest energy. The whole excitation process requires less than 10^{-12} sec [5]. From the first excited singlet level, the molecule may decay by one of three major pathways: it may drop back to the ground state by emitting radiation of a wavelength longer than that of absorption; it may drop back without emitting radiation, or it may undergo intersystem crossing to the first excited triplet state (T_1). The first process is an important spectroscopic process requiring about 10^{-9} sec [6] and is called fluorescence. Qualitatively, the fluorescence spectrum is the mirror image of the absorption spectrum [17]. However, since absorption may occur to any one of a number of excited states above the first, the absorption spectrum of a molecule generally contains some structure on the short wavelength side of the absorption maximum.

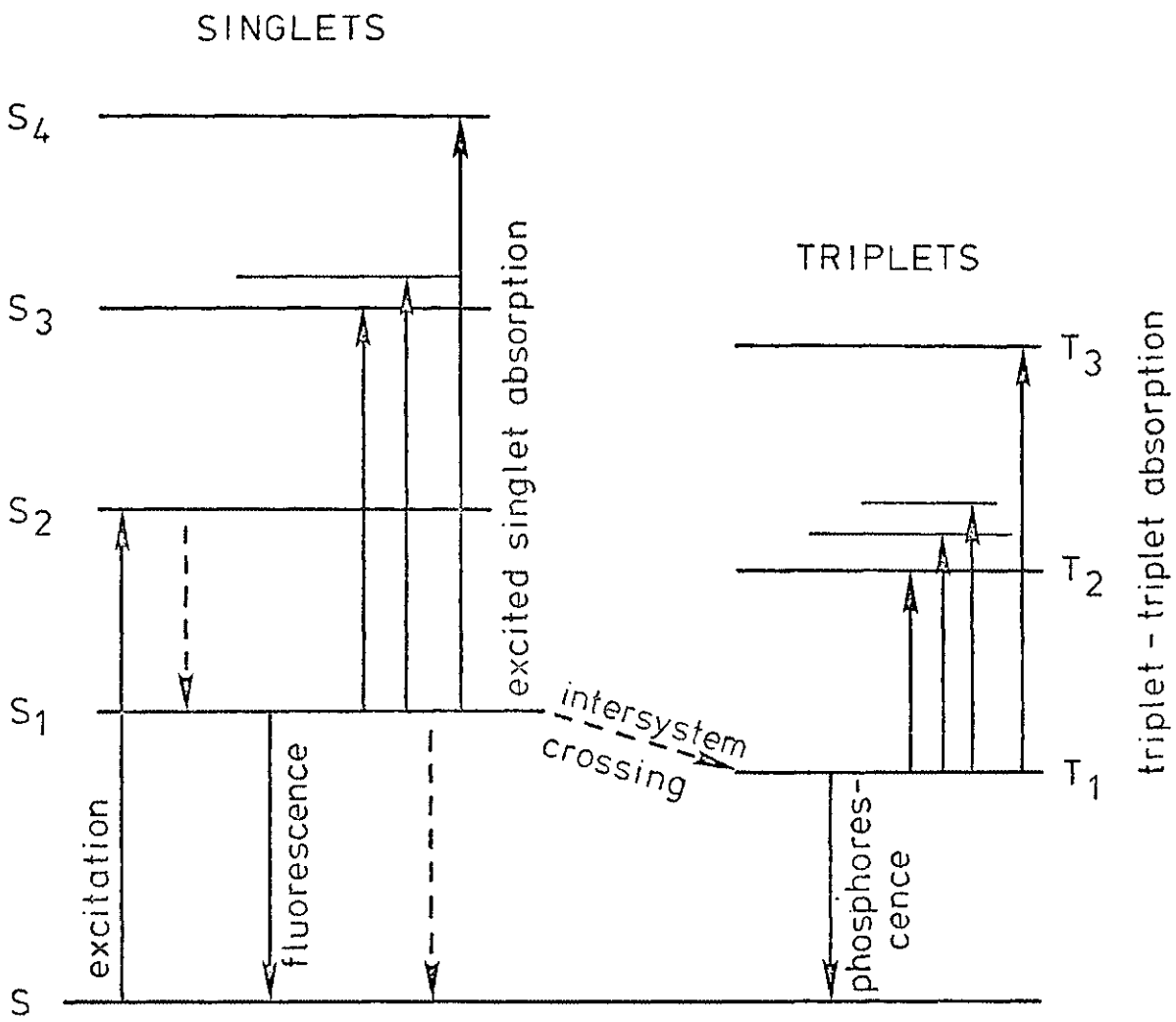

Figure 2-1. A simple diagram showing the energy transitions when a molecule is pumped

Degradation from the first excited singlet state is not limited to fluorescence. Generally, the potential energy surfaces associated with the first singlet state and with the excited triplet state intersect [8]. At some time, the nuclear configuration of the first singlet state and the first triplet state as well as the potential energy of the two states are exactly the same. At this instant, the molecule may cross, without radiation, from the first excited singlet state to the first excited triplet state. This radiationless conversion is called intersystem crossing and the rate K_{isc} is typically about 10^{-7} sec [16].

The first excited triplet state is generally of lower energy than the first excited singlet state. Therefore, intersystem crossing is an energetically downhill process. Since singlet-triplet conversions are low probability transitions, the triplet state is decidedly more stable (has a longer lifetime) than the singlet state. However, after a time period, which varies from 10^{-6} sec to several minutes [18], the triplet state also decays to the ground state. When it does so, a photon of light may be emitted, but its wavelength is substantially longer than the wavelength of the radiation initially absorbed (because of the lower energy of the triplet state). This process is called phosphorescence.

Because of the comparatively long lifetime of the triplet state, the majority of photochemical reactions

occur from this excited state. It is the reason why photophysicists and photochemists are so interested in the molecula triplet state.

Related Experiments

Lewis [18] was the first to investigate the triplet spectra of some organic materials. He used a mercury lamp to pump the test molecules which he put in a rotating can mounted on a variable speed motor. A section was cut out, about a third of the way around the can, so that the sample was alternately illuminated and viewed by the spectroscope which was on the other side. Figure 2-2, shows the arrangements of Lewis experiment. This observation was limited by the speed of the motor; it had a milli second resolution. Such an experimental arrangement was improved by Porter [20]. He used the same pumping source as Lewis but the sample cell was fixed, and a spectrograph was placed at the other end. Between the sample cell and spectrograph was a chopper responsible for synchronization of the shutter. This method had a higher resolution, up to the micro second range. However, in order to produce an image on the photographic plate in a short time from a source of continuum, one needs either a strong source or has to resort to a large number of short exposures. The latter might result in a high decomposition rate, and because the high energy makes it necessary to cool the

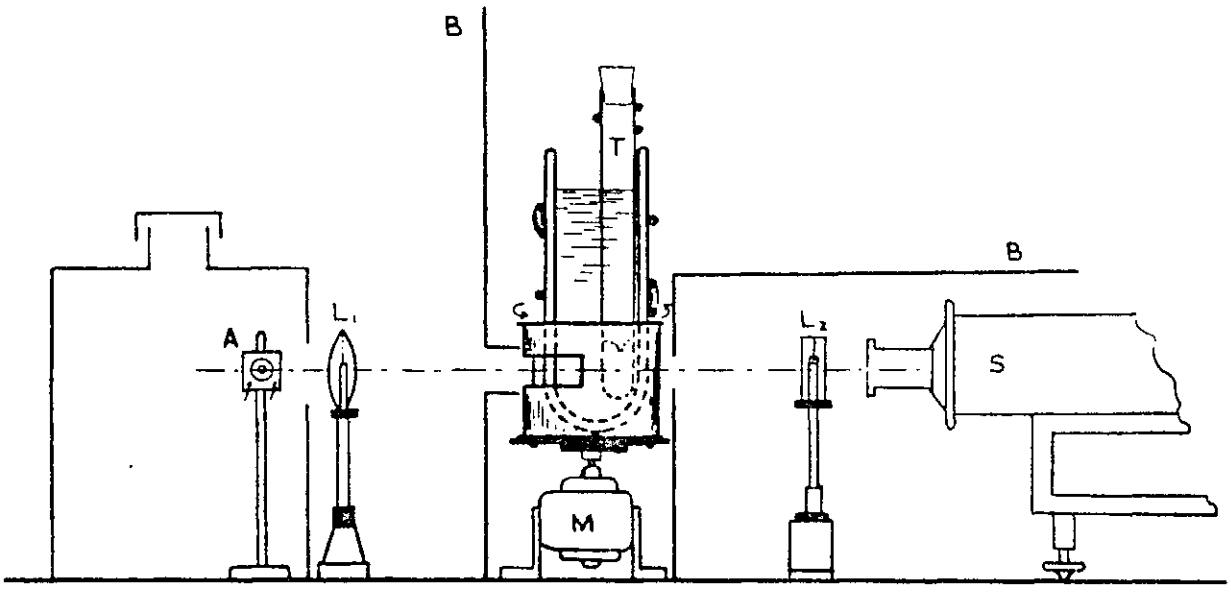

Figure 2-1. The Lewis experiment

(A) Mercury lamp (B) Blackened cardboard

(C) Sample tube (L) Focus lens

(T) Containing the solution to be studied

lamp between flashes, such an experiment takes a long time to complete.

In 1968, Novak and Windsor [21] applied the ruby laser as a pump in an experiment. The advent of the laser provided the chemist with a light source which is monochromatic, having a short duration and great intensity-many orders of magnitude more powerful than any previous flash lamps. However, at that time, the use of the laser in photochemical experiments was limited. One reason was that most availiable lasers, at that time, operated in the visible or infrared and so were not useful as photochemical sources.

In our laser pump and probe experiment, a multiline excimer laser was used as a pump source. It lases at many different wavelengths from 157 nm (F_2) to 10,600 nm (CO_2). Also, our probe beam is a pulsed tunable dye laser with continuous probe wavelength from 324 nm to 600 nm. The experiment could conceivably be extended to pulse widths in the hundreds of picoseconds [22].

Contact Charge Transfer Lasers

A long-term goal of our experiment is search for new laser sources, the Contact Charge Transfer Lasers. Some theoretical research, based on earlier work by Mulliken and coworkers [30,31], has been done by Dharamsi [9,23,25,26].

It has been known for several years now that even valence saturated atoms and molecules interact with one

another [27]. This kind of interaction is responsible for the formation of molecular complexes whose existence was discovered when absorption spectra, not exhibited by either component alone, were found when two different molecules interacted [28,29].

Molecular complexes of this type themselves vary in bounding energies. Absorption spectra have been measured for very stable complexes as well as for complexes which have practically no binding energy in ground state. In the latter case the components are merely "in contact" in Mulliken's terminology [54]. These contact charge transfer complexes are also called electron donor-acceptor complexes, because the force is from the electronic charge transfer between the interacting components, one of which is an electron donor while the other is an acceptor. A possible scheme for creating contact charge transfer complexes is by using an excited triplet state donor molecule in collision with an acceptor molecule. Because there is no binding energy in ground state, once the contact charge transfer complexes are formed population inversion is obtained. This mechanism is illustrated in figure 2-3.

The next chapter describes the experimental arrangement used in our work.

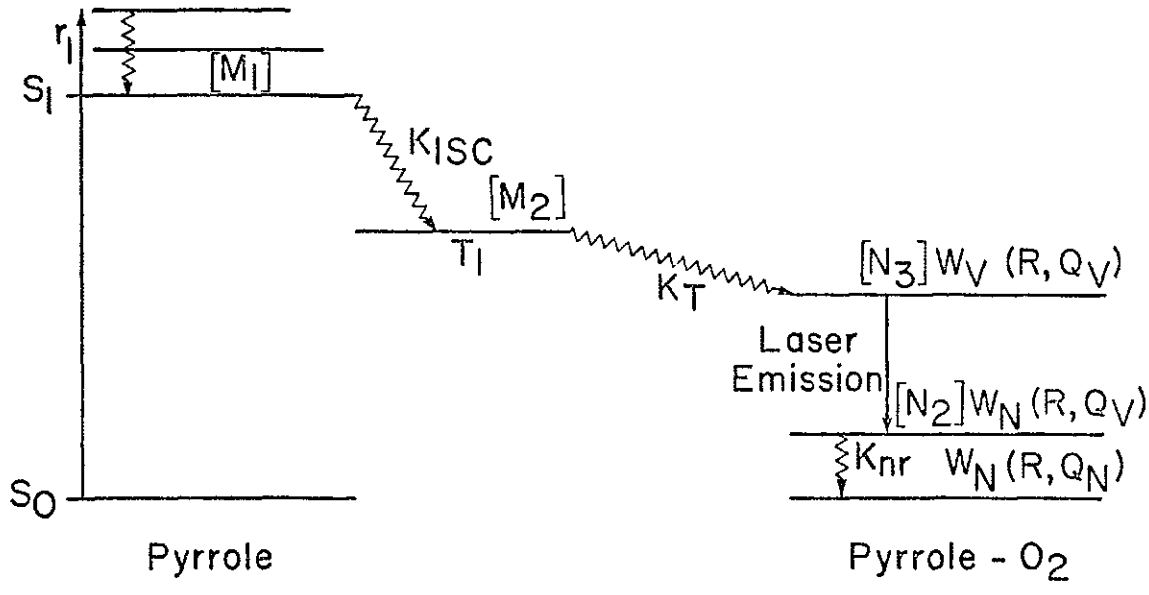

Figure 2-3. Mechanism of contact charge transfer complexes

Chapter III

EXPERIMENTAL ARRANGEMENT

The experimental apparatus used is shown schematically in Figure 3-1.

A multiline excimer laser (Tachisto 801XR) was operated on the 248 nm line of KrF. This radiation was divided by a beam-splitter with about five percent going to pump a dye laser (Molectron DL-10) while the remainder was incident on a quartz sample cell. The probe dye laser was brought into the cell in a direction orthogonal to that of the pump beam, after reflecting from several mirrors (M1 - M5). The fact that the probe dye laser and sample were pumped by the same excimer pulse ensured a jitter-free pump-probe delay. Time resolution was obtained by changing the optical path difference between the pump and probe beams to the sample cell. This was accomplished simply by changing the locations of the delaying mirrors. Each pump-probe delay was measured directly on a fast oscilloscope (Tektronix 7904).

The optical signals were wavelength-resolved by a monochromator (ISA Model HR-320) containing a 1200

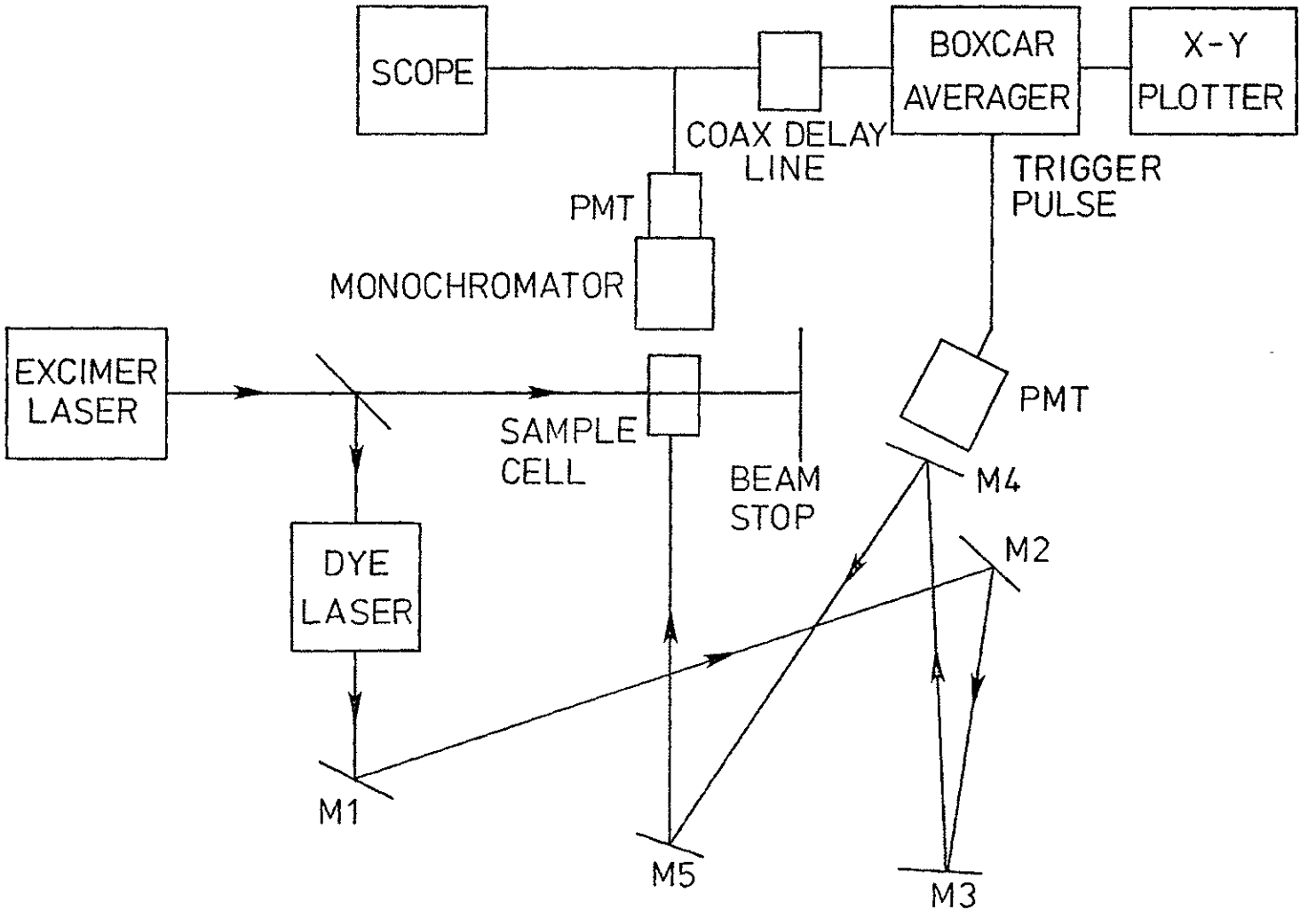

Figure 3-1. Schematic diagram of experimental apparatus

groves/mm holographically ruled diffraction grating. These signals were then detected by a fast end-on photomultiplier tube (Hamamatsu R2055, with a rise time < 800 ps), and fed into a model 166 Gated Integrator module of a boxcar averager (Princeton Applied Research Model 162). The latter was triggered optically by a part of the probe dye laser pulse, ensuring a jitter-free interval between the gate sampling pulse and the signal. The internal dead-time of the boxcaraverager (i.e. the delay between its trigger and sampling pulses) was compensated for by delaying the electrical signal from the PMT through a roll of impedance-matched coaxial cable. The signals were monitored on the oscilloscope and recorded on an X-Y plotter. It was found that the coaxial cable delay line, while stretching out the pulses somewhat, also served as an effective filter for the transient r-f noise that was produced by the pulsed-power circuit of the excimer laser.

Pumping Source - Excimer Laser

The pumping system used was an excimer laser (Tachisto 801XR, see Figure 3-3 A) which is a multi-gas pulsed laser of advanced design, primarily intended for use as a Rare Gas Halide excimer laser. Nominal operating specifications are given in Table III-1.

Table III-1 Multiline characteristics of the excimer laser

Medium	ArF	KrF	XeCl	XeF
Wavelength (nm)	193	248	308	300
Max. Energy (mj)	400	750	400	300
Max. Average Power(watts)	6	12	7.5	6
Life time(shots)	$1x10^5$	10^6	$6x10^6$	$3x10^6$

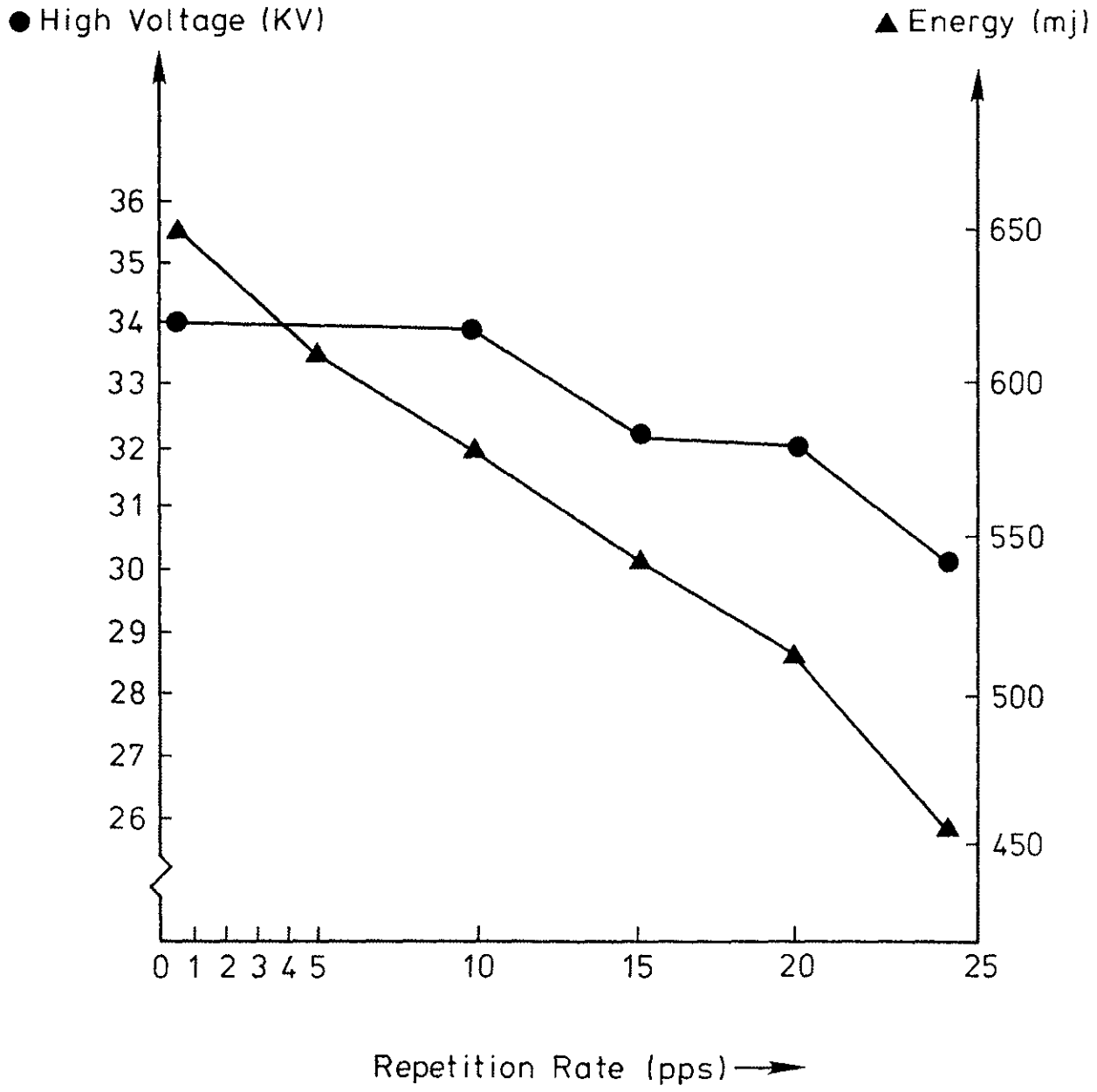

Figure 3-2. Operation parameters of KrF excimer laser

The excimer laser used a transverse electric discharge, formed between two profiled electrodes, to excite mixtures of rare gases and halogens. In the discharge, rare gas halide excimers are formed. These are compounds which are only bound in the excited state. The ground states of excimer are bound, or very weakly bound. The excited temporary state returns to the ground state by radiative transition and, in doing so, emits a UV photon. The photon energy is dependent upon the particular excimer species.

The maximum laser energy output was generally obtained at a repetition rate less than 10Hz and high power supply voltage. Figure 3-2, shows the operational parameters for this excimer laser operating on the KrF (248 nm) line.

Each excimer mixture has associated with it a characteristic lifetime to 50% energy. Lifetime can be improved upon by pumping the system down to approximately 10^{-3} torr and obtaining maximum passivation.

Dye Laser Characteristics Under 248 nm Pumping

As mentioned before, the dye laser (Molectron DL-10, see Figure 3-3 B) has a small quartz dye cell which hold the dyes. Most dye lasers are pumped by the XeCl (308 nm) or N_2 (337 nm) lines. However, our experiments required a 248 nm pump for both the sample and dye laser. In order to accomplish this, some experimentation regarding the suitability of all the dyes under a 248 nm pump was

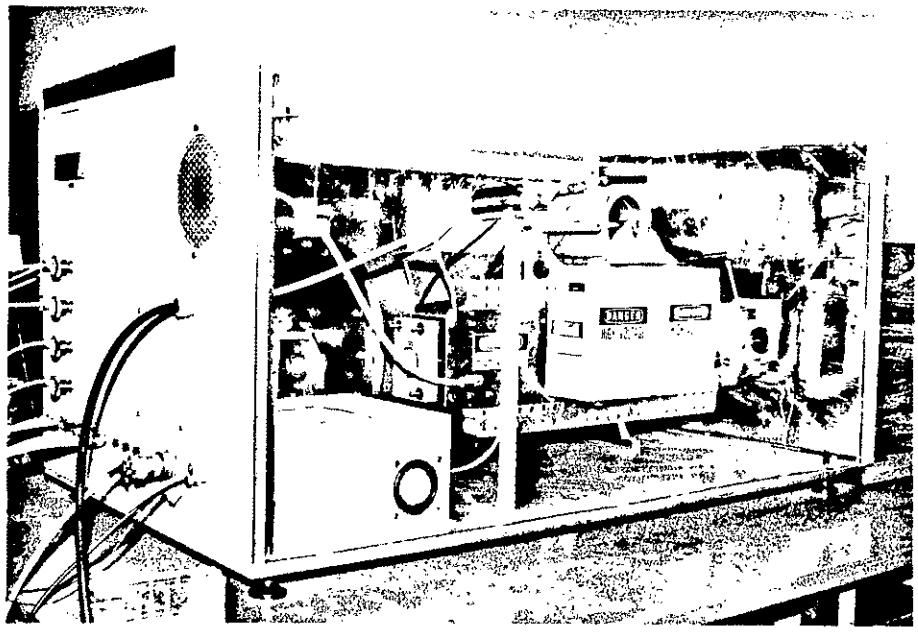

(A)

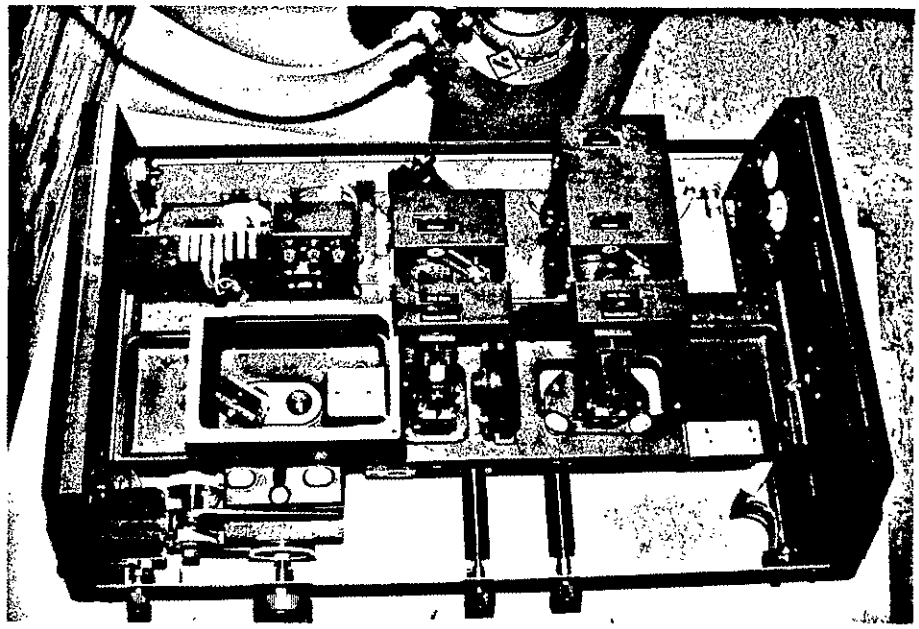

(B)

Figure 3-3. (A) Tachisto 801 XR excimer laser
(B) Molectron DL-10 dye laser

Table III-2 The Laser Dyes which Lased Well in Our System

DYE	Solvent	Concentration	Lased Range(nm)
DMT	1,4 dioxane	5×10^{-3} M	324 - 343
DMT	cyclohexane	5×10^{-3} M	324 - 332
TMO	cyclohexane	4×10^{-3} M	350 - 364
α-NPO	1,4 dioxane	3×10^{-3} M	352
BPBD-365	cyclohexane	5×10^{-3} M	360 - 380
PBD	cyclohexane	5×10^{-3} M	362
LD-390	cyclohexane	5×10^{-3} M	380 - 385
PBBO	cyclohexane	5×10^{-3} M	394 - 402
LD-423	ethanol	5×10^{-3} M	410 - 423
POPOP	1,4 dioxane	2×10^{-3} M	414 - 423
BIS-MSB	1,4 dioxane	5×10^{-3} M	418 - 425
C-440	ethanol	5×10^{-3} M	422 - 453
C-450	ethanol	1×10^{-2} M	436 - 459
C-460	ethanol	1×10^{-2} M	450 - 480
7D4TMC	1,4 dioxane	Molectron 70368-2	470 - 512
C-485	ethanol	Molectron 70371-2	505 - 552
C-495	ethanol	Molectron 70369-2	523 - 582
R6G	ethanol	Molectron 70360-2	580 - 610

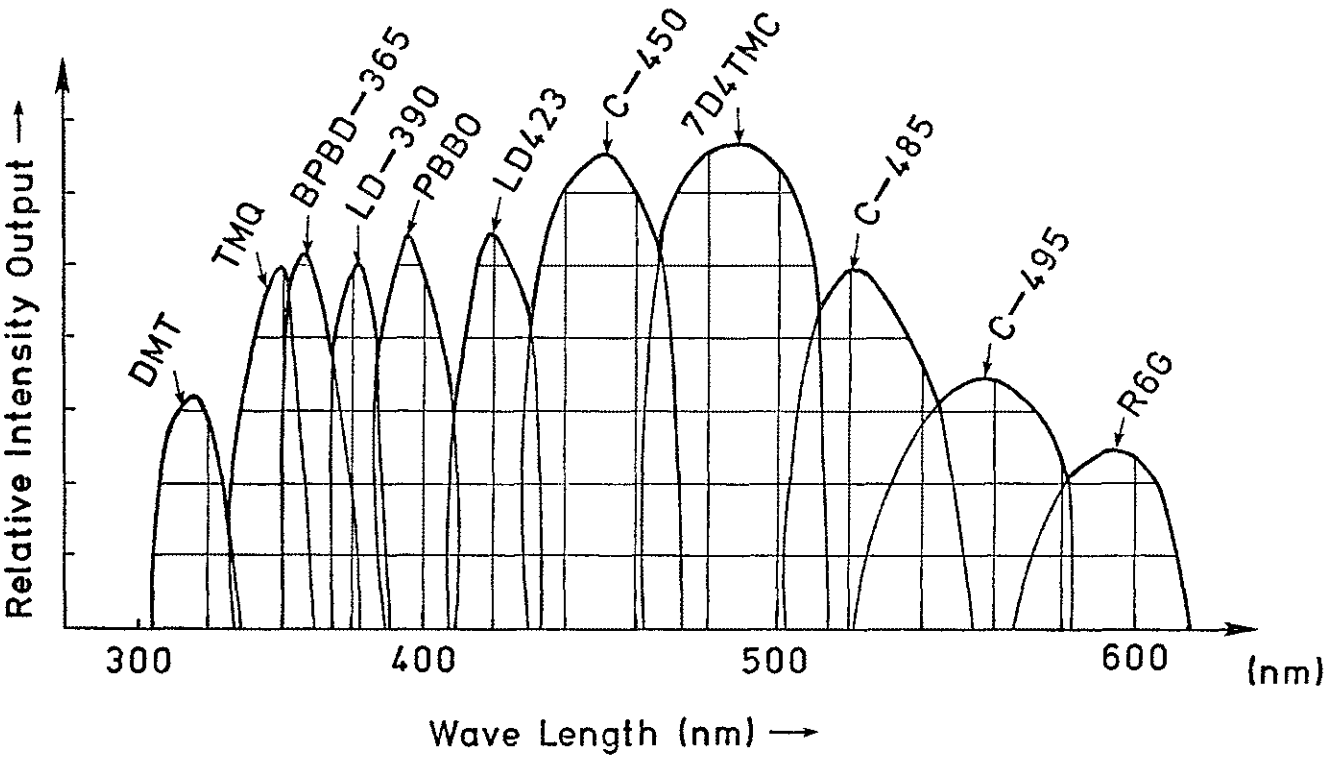

Figure 3-4. KrF (248 nm) excimer laser-pumped dyes relative intensity output versus wavelength

undertaken. Table III-2 lists those dyes that lased at particular wavelengths, together with the solvent and concentration. All these lased strongly enough to be recorded with Δ t = 100 ns (5 mirrors). Figure 3-4 shows the most frequently used dyes and relative intensity output versus wavelength under 248 nm pump. These dyes are DMT (in 1,4 dioxane and cyclohexane), TMQ (in cyclohexane), α-NPO (in cyclohexane), PBD (in cyclohexane), BPBD-365 (in cyclohexane), LD-390 (in cyclohexane), PBBO (in cyclohexane), LD-423 (in ethanol), POPOP (in 1,4 dioxane), BIS-MSB (in 1,4 dioxane), Coumarin-440 (in ethanol), Coumarin-450 (in ethanol), Coumarin-460 (in ethanol), 7D4T-MC (in 1,4 dioxane), Coumarin-485 (in ethanol), Coumarin-495 (in ethanol), Rhodamine6G (in ethanol), which yield an almost continuous probe wavelength from 324 nm to 600 nm.

Vacuum System And Sample Cell

For experiments in the gaseous form, a vacuum system (Edwards-100) was chosen, which incorporates a diffusion pump, a water cooled baffle, a trap, an isolation valve, a backing valve and a by-pass valve. Above this, a glass-made sample cell was set (see Figure 3-5 A), the sample cell being 3 inches in diameter and 8 inches in height, with four quartz windows and four nipples. The molecular samples inside were pumped by the excimer radiation going through two large windows (2 inches diameter), and probed orthogonally by the dye laser pulse

going through two windows (1 inch diameter). The probe signal passed through the monochromator and was detected by the PMT which was connected to the scope. The sample cell has four ports connected to a Penning pressure gauge (Edwards Penning 8) which could measure pressures down to 10^{-7} mbar, and the other was connected to a capacitance manometer gauge (MKS 222AB) with digital readout which measured the tested molecular pressure, from 0.1 torr up to 1000 torr, the last two ports served for feed through connections. Figure 3-5 shows the glass test tube-stopcock arrangement used for introducing samples which were liquids at room temperature and pressure. In use, valve 1 was closed first and the liquid introduced in tube A, valve 2 was opened and tube B was evacuated, and then valve 2 was closed and valve 1 opened gradually to let some liquid flow into the tube B. Finally the valve was closed. Valve 2 was used to control the input pressure. Liquid in tube B vaporized and entered the system.

Figure 3-6 shows photographs of the experimental arrangement for the vapor phase experiments.

For liquid samples, the arrangement was much simpler, requiring only a quartz cell with four polished sides, a beam entering through two opposite windows and a dye laser pulse passing through the other walls.

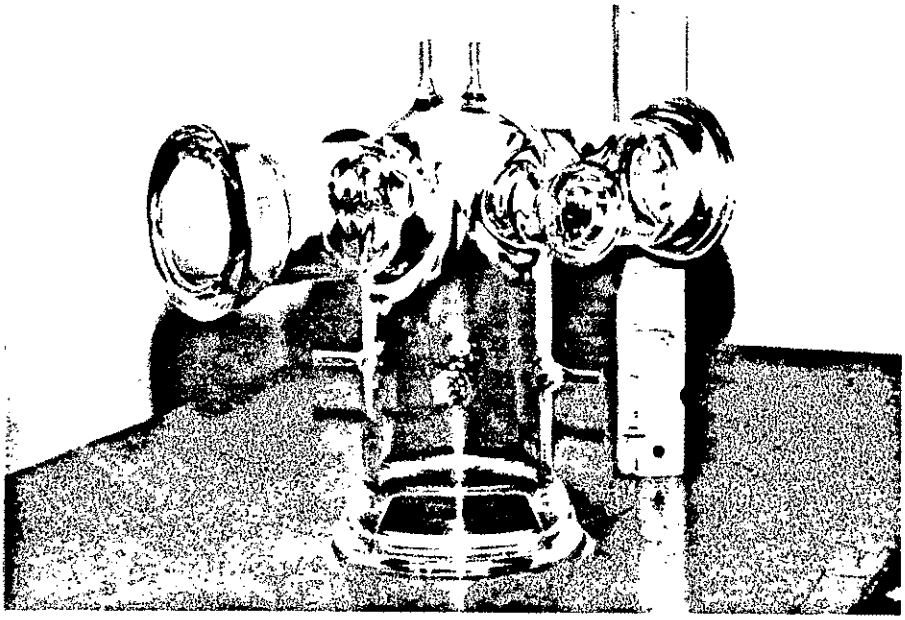

(A)

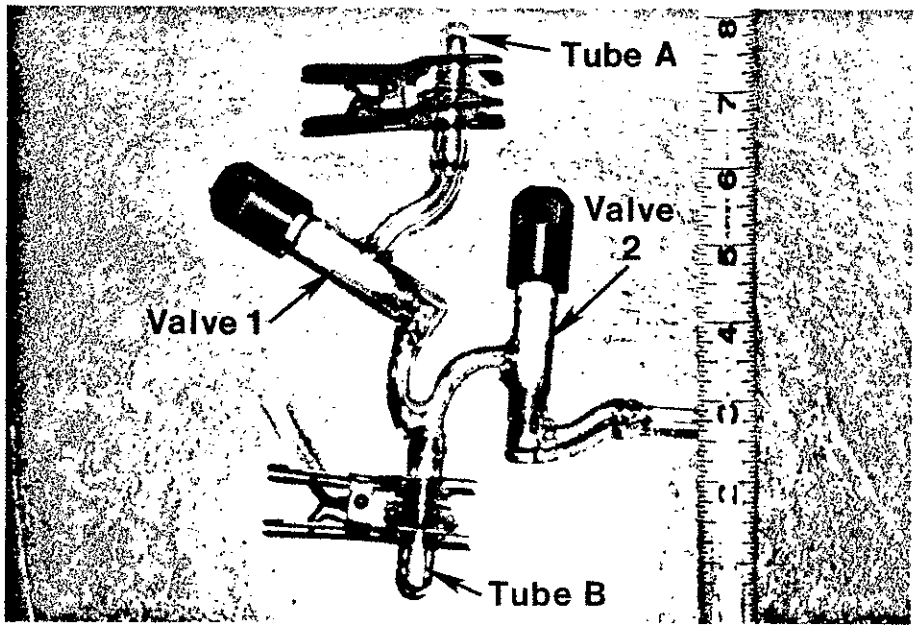

(B)

Figure 3-5. (A) Sample cell for vapor phase experiments
(B) Arrangement for introducing liquids
into gaseous sample cell

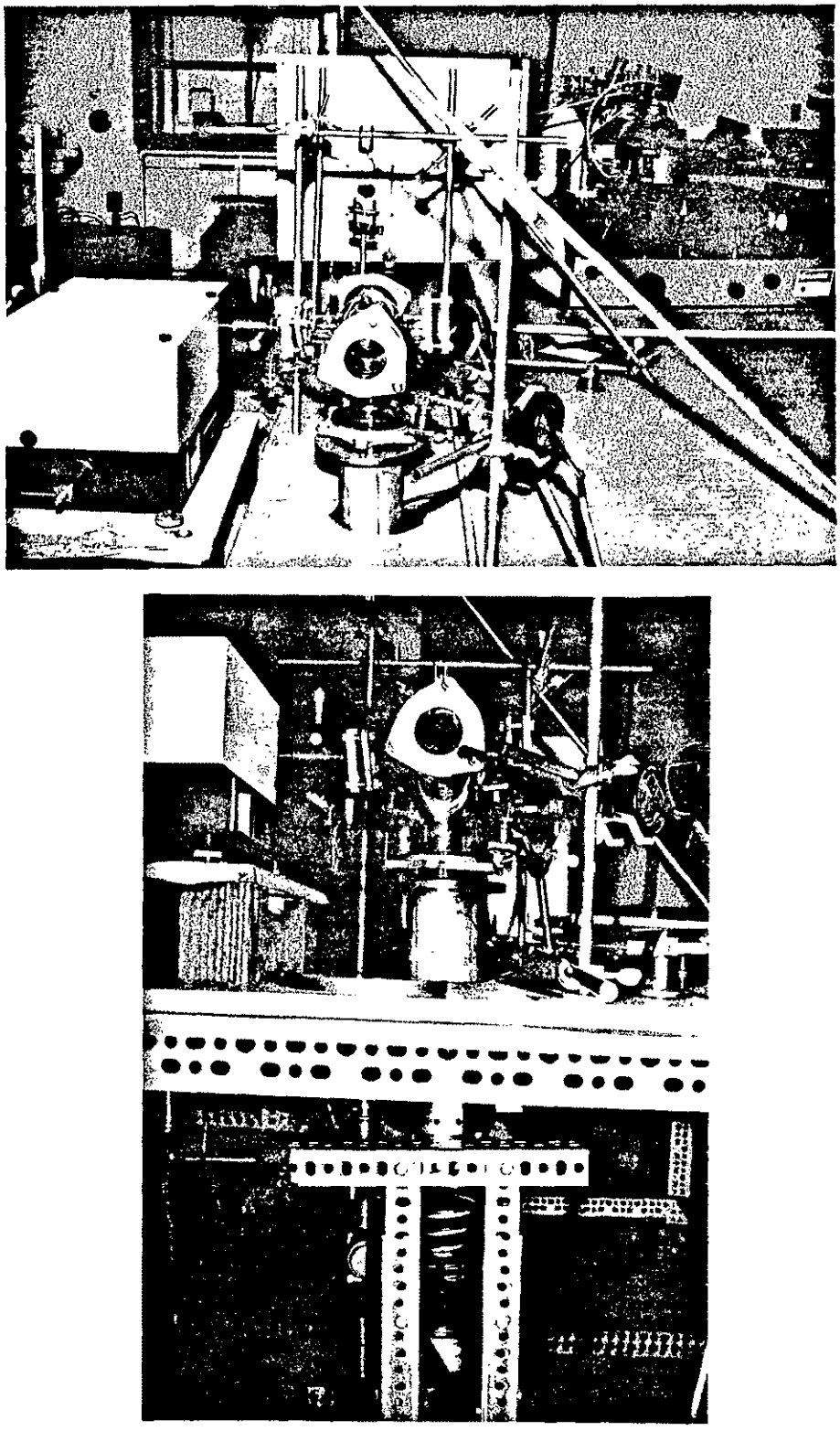

Figure 3-6. Photograph of apparatus used in vapor phase experiments

Boxcar Averager

The boxcar averager is a versatile gated integrator used for the measurement of repetitive signals. Basically, the technique involves repetitively gating out a particular section of a waveform and integrating the gated signals to improve the signal-to-noise ratio (S/N). It is particularly useful for measuring respective short pulse signals and signals that have a slow repetition rate or low duty cycle. In our experiment, the highest repetition rate was 11 Hz and the pulse widths of both dye and excimer lasers were in the nano second range. Because the signals fluctuate and were noisy, a boxcar averager (Princeton Applied Research Model 162) was used to measure the average of many shots.

This system synchronously samples the input signal with an aperture that can be fixed at any point on, or slowly scanned across, the input signal. The signal passed through the aperture is applied to a variable time constant integrator, the output of which is the average of some number of repetitions of the input signal over the aperture duration. Because the average value of noise over a large number of repetitions is zero, an improvement in signal-to-noise ratio occurs. The output is connected to an X-Y plotter to obtain a hard-copy record (see Figure 4-1, in chapter IV).

Photo-Multiplier Tube (PMT)

The photomultiplier tube (PMT) is a photosensitive device consisting of a photoemissive cathode followed by a focusing electrode, an electron mutiplier and an electron collector, i.e., an anode in a vacuum tube, as shown in Figure 3-7(a).

When light enters the photocathode, it emits photoelectrons into the vacuum of the photomultiplier. The number of photoelectrons emitted from the photocathode is proportional to the number of incident photons. These photoelectrons are then directed by the focusing electrode voltages towards the electron mulitiplier where they are multiplied by the process of secondary emission. The secondary electrons are collected by the anode and registered as the output signal.

Figure 3-7(b) is a photograph of the R2055 (Hamamatsu) photomultiplier tube which was used in the experiment. It has a gain of 1×10^6 when operated at 1250 V, and a rise time of 0.6 ns(at 1250 V), the spectral response being from 160 nm to 650 nm. Figure 3-8 shows two single photo-electron time distributions spaced 3 ns apart of this photomultiplier tube, which indicates the speed of the time response [26].

The individual devices that were used have been described above. The next chapter describes the experiments performed and the results obtained.

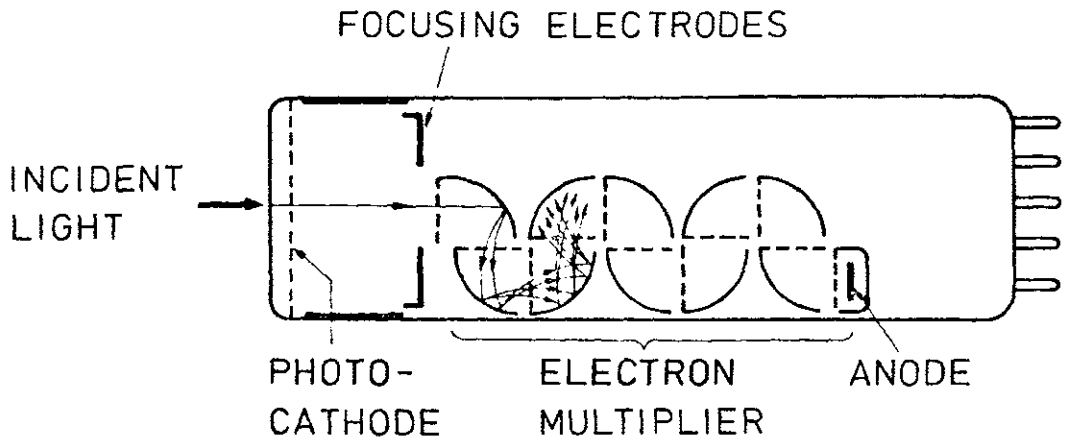

(A)

(B)

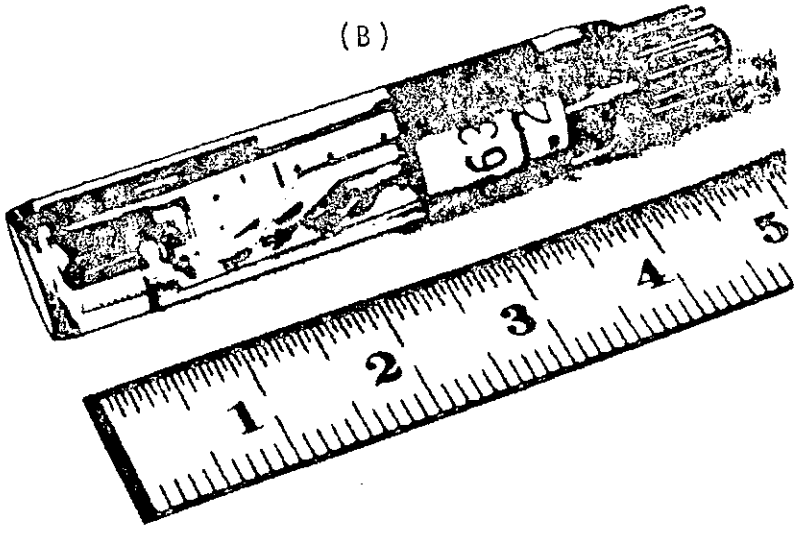

Figure 3-7. (A) Photomultiplier tube
(B) Photograph of R 2055 PMT

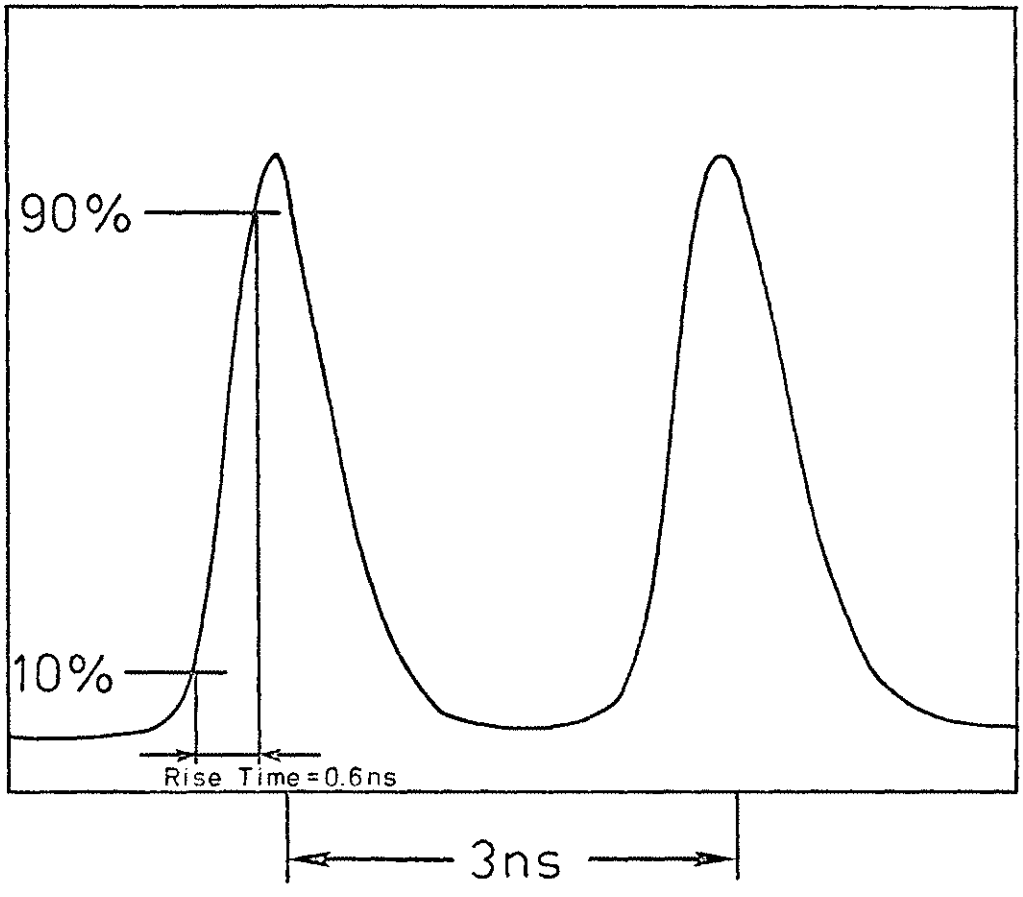

Figure 3-8. Two single photoelectron time distributions and the rise time of R 2055 PMT

Chapter IV

EXPERIMENTAL PROCEDURE AND RESULTS

In this chapter, a procedure for experiments carried out in both the liquid and vapor phases is described and their results presented. Some experiments were performed with a borrowed boxcar average; others were not.

Experiments For PPO (2,5 Diphenyloxazole)

For those experiments with a boxcar averager, a sample hard-copy record from the X-Y plotter is presented in Figure 4-1. The procedure consisted of recording (a) the dye laser probe-pulse with the excimer radiation blocked off from the sample cell, (b) the signal with the dye pulse blocked off, but with the excimer incident, and (c) the signals with both the pump and probe radiation incident on the sample. Each measurement, corresponding to a given probe wavelength at a certain pump-probe delay time Δt, was performed with the boxcar averaging for about 40 seconds in the scanning mode, and with the excimer laser firing repetitively at 10Hz, which means each record took the average value of approximately 400 shots. It was important to perform this type of averaging because the excimer laser, and consequently the dye laser also, varied in

intensity from shot to shot. A fresh sample of tested solution was used for every run.

Experiments using this method were performed on solutions of PPO in cyclohexane, 1,4 dioxane and toluene for several values of the pump-probe delay time Δt, several probe wavelengths between 330 nm to 530 nm and several different concentrations. All measurements were performed at room temperature. Laser grade PPO obtained from Exciton, cyclohexane (Fisher, spectra-analyzed), 1,4 dioxane (Fisher, certified ACS), and toluene (Fisher, spectra-analyzed), were used without further purification.

Experiments were performed with air-equilibrated solutions, as well as with deoxygenated (by bubbling 99.998% pure N_2) solutions. Some experimental runs were also performed with oxygen-saturated (by bubbling 99.996% pure O_2) solutions. Control exeperiments using the solvents alone were also performed.

A typical set of plots obtained on the X-Y plotter is shown in Figure 4-1. This shows the signals for a given run with (a) the excimer radiation blocked off but the dye probe incident on the sample (b) the dye laser blocked off but the excimer signal incident and (c) with both excimer-pump and dye-probe pulses incident on the sample.

Figure 4-1(a) is the probing dye laser pulse which has a full-width-at-half maximum (FWHM) of about 20 ns, being somewhat narrower than the excimer pulse. Figure 4-1 (b) is part of the $S_1 \longrightarrow S_0$ fluorescence band of PPO

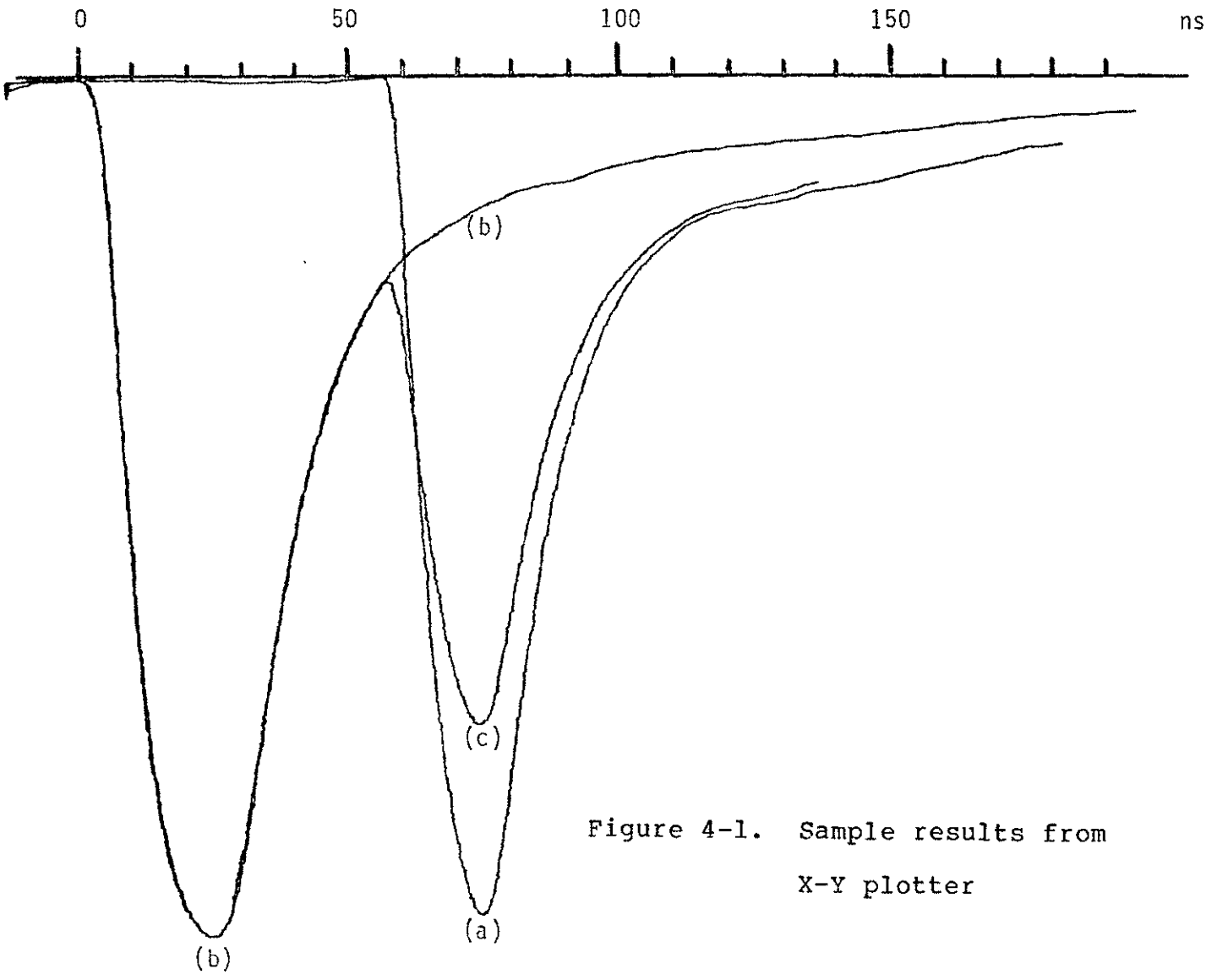

Figure 4-1. Sample results from X-Y plotter

which extends from 340 nm to 510 nm [10]. This signal followsthe temporal profile of the 248 nm pump because the latter has a FWHM of approximately 30 ns, whereas the S_1 state of PPO has a fluorescence lifetime of about 2.0 ns [11,12]. The rate of optical excitation of the singlet state of PPO by the 248 nm radiation is therefore the limiting process here. Figure 2(c) is the resultant signal from the PMT when both the pump and dye lasers are incident on the sample.

Excited-State absorption was calculated by Lambert's law [13] mentioned in chapter II:

$$I = I_o \exp(-n\sigma d)$$

$$U_d = n\sigma d = -\ln(I/I_o)$$

where U_d is the absorption coefficient.

In Figure 4.1, I_o is sum of (a) and (b), and I is (c), Table IV-1 is a set of measured data at Δt = 45 ns . Table IV-2, and Table IV-3 are for Δt = 75 ns and 100 ns respectively. The absorption versus probe wavelengths for these three time-resolved measurements are plotted in Figure 4-2 (a), (b), and (c). The absorption seems to peak around 400 nm.

Figure 4-3, shows the results of excited state absorption measurements on solutions of PPO in cyclohexane at 476 nm, 418 nm, and 402 nm, taken with Δt = 100 ns. Consistent with the results shown in figure 4-2, the absorption increases progressively from 476 nm to 402 nm, for all concentrations investigated. A concentration

Table IV-1 Excited State Absorption For PPO in Cyclohexane at Concentration 5×10^{-3} M, with 248 nm Pump: Probe Delay Time $\Delta t = 45$ ns.

Probe Wavelength (nm)	I_o	I	$-\ln(I/I_o)$
329	5.8	5.3	0.09
336	7.9	7.1	0.11
340	6.1	5.7	0.07
345	8.3	7.2	0.14
352	13.9	10.7	0.26
356	15.6	11.5	0.30
361	15.3	11.4	0.29
366	15.3	11.4	0.29
370	15.5	11.8	0.21
377	12.3	9.1	0.30
380	15.0	11.3	0.28
385	15.4	11.0	0.34
394	16.6	11.6	0.36
398	14.9	11.8	0.23
402	14.3	10.6	0.30
407	15.1	11.1	0.31
414	11.8	9.3	0.24
419	15.1	12.5	0.19
425	14.2	11.8	0.19
430	14.8	11.7	0.24
435	14.1	11.6	0.20
440	16.4	13.1	0.23
450	16.4	13.2	0.22
460	15.0	12.9	0.15
470	14.1	12.3	0.14
480	14.8	13.0	0.13
490	14.6	13.1	0.11
501	14.0	13.0	0.74

Table IV-2 Excited State Absorption For PPO in Cyclohexane at Concentration 5×10^{-3} M. with 248 nm Pump; Probe Delay Time $\Delta t = 75$ ns.

Probe Wavelength (nm)	I_0	I	$-\ln(I/I_0)$
399	9.7	5.7	0.53
437	14.9	10.5	0.35
444	14.8	10.1	0.38
452	15.1	11.0	0.32
461	15.4	11.7	0.28
470	11.5	9.2	0.22
476	11.7	8.5	0.32
480	13.1	10.2	0.25
494	13.0	10.5	0.21
504	12.8	10.7	0.18
511	13.2	11.2	0.16

Table IV-3 Excited State Absorption For PPO in Cyclohexane at Concentration 5×10^{-3} M. with 248 nm Pump; Probe Delay Time $\Delta t = 100$ ns.

Probe Wavelength (nm)	I_o	I	$-\ln(I/I_o)$
370	4.7	2.9	0.48
380	3.6	2.2	0.49
400	8.5	4.2	0.71
404	9.5	5.3	0.58
416	10.8	5.8	0.65
421	11.8	7.8	0.41
429	9.7	5.5	0.57
434	14.6	9.3	0.45
441	14.8	9.9	0.42
451	15.0	10.3	0.38
461	14.2	9.7	0.38
468	9.7	5.6	0.55
481	9.7	6.7	0.37
504	13.3	10.4	0.25
515	11.8	9.2	0.21

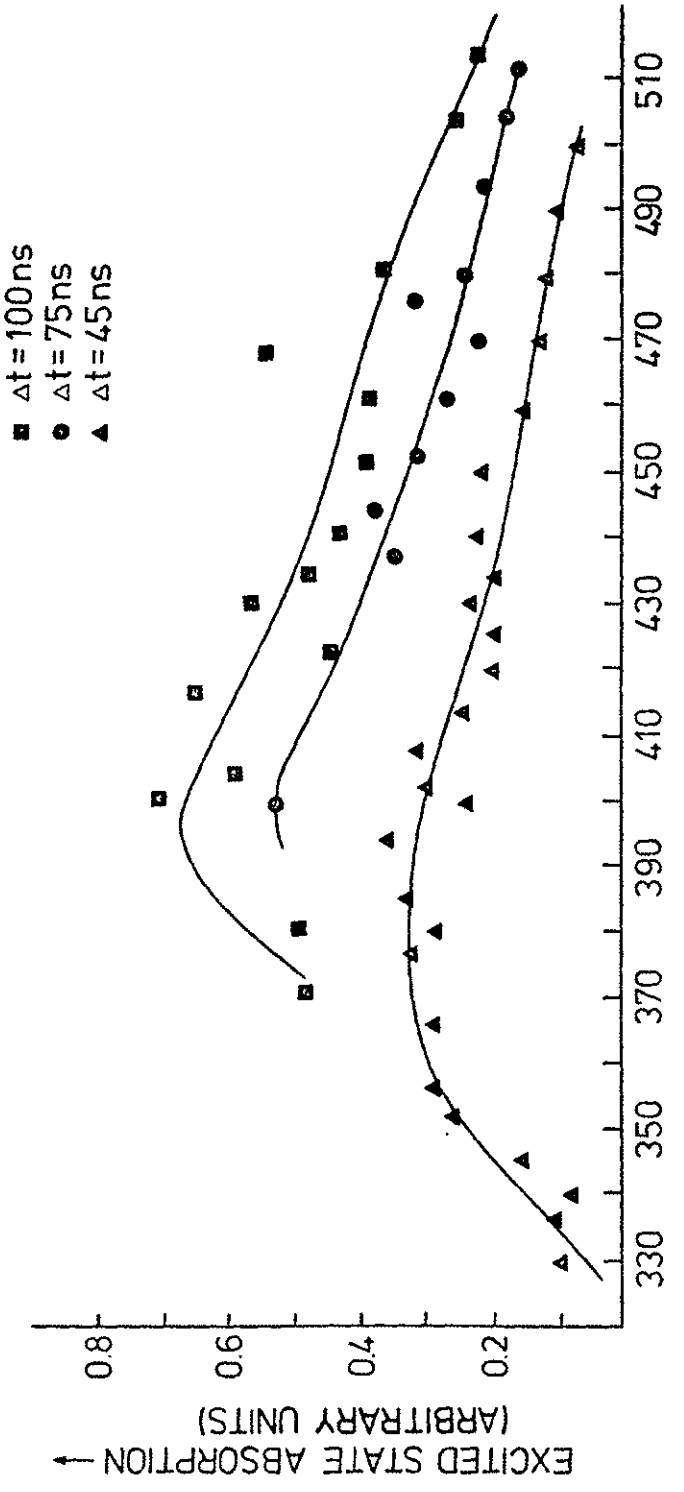

Figure 4-2. Excited state absorption measurements with various delay times for PPO solution (5×10^{-3} M) in cyclohexane

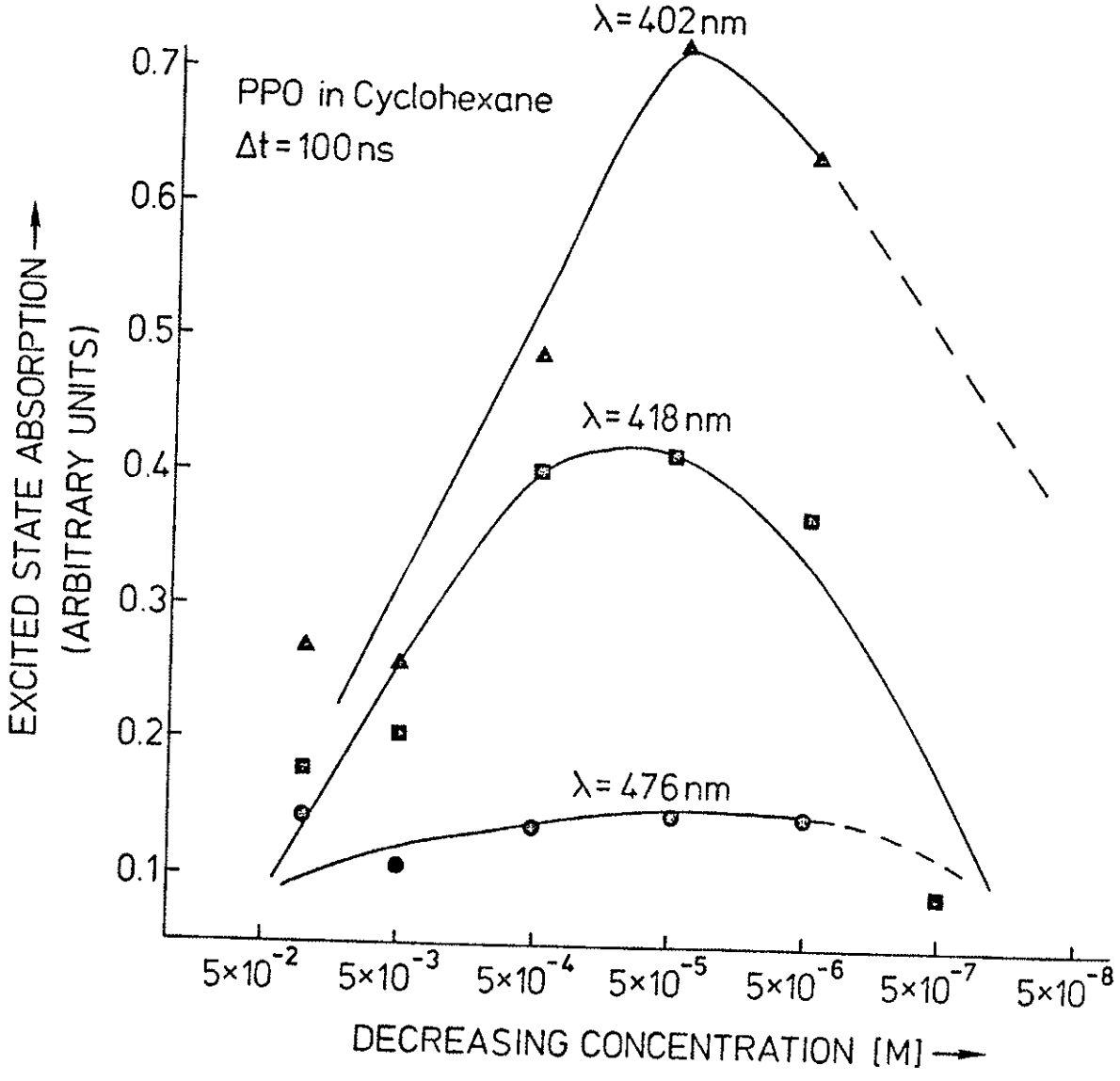

Figure 4-3. Excited state absorption for PPO in cyclohexane as a function of concentration at 476, 418, and 402 nms with Δt = 100 ns

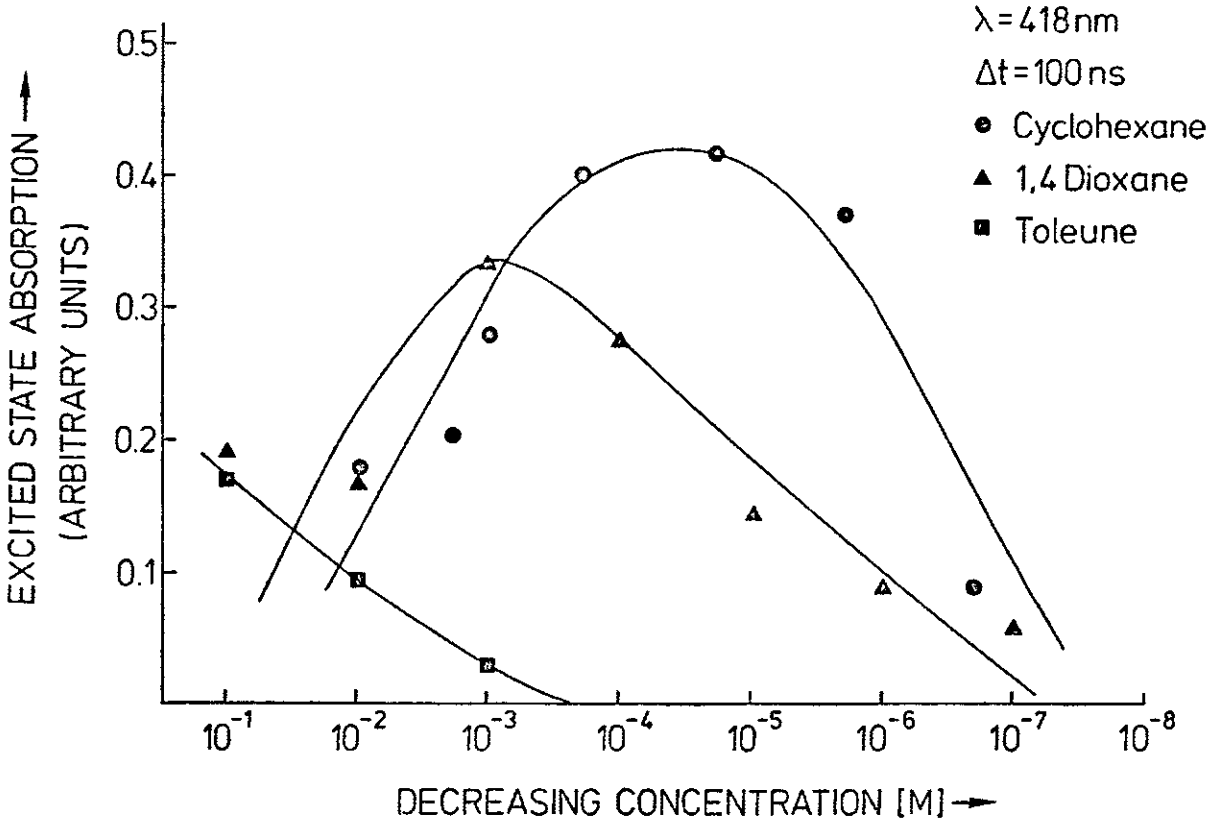

Figure 4-4. Excited state absorption as a function of concentration for PPO in cyclohexane, 1,4 dioxane, and toluene at Δt = 100 ns λ = 418 nm

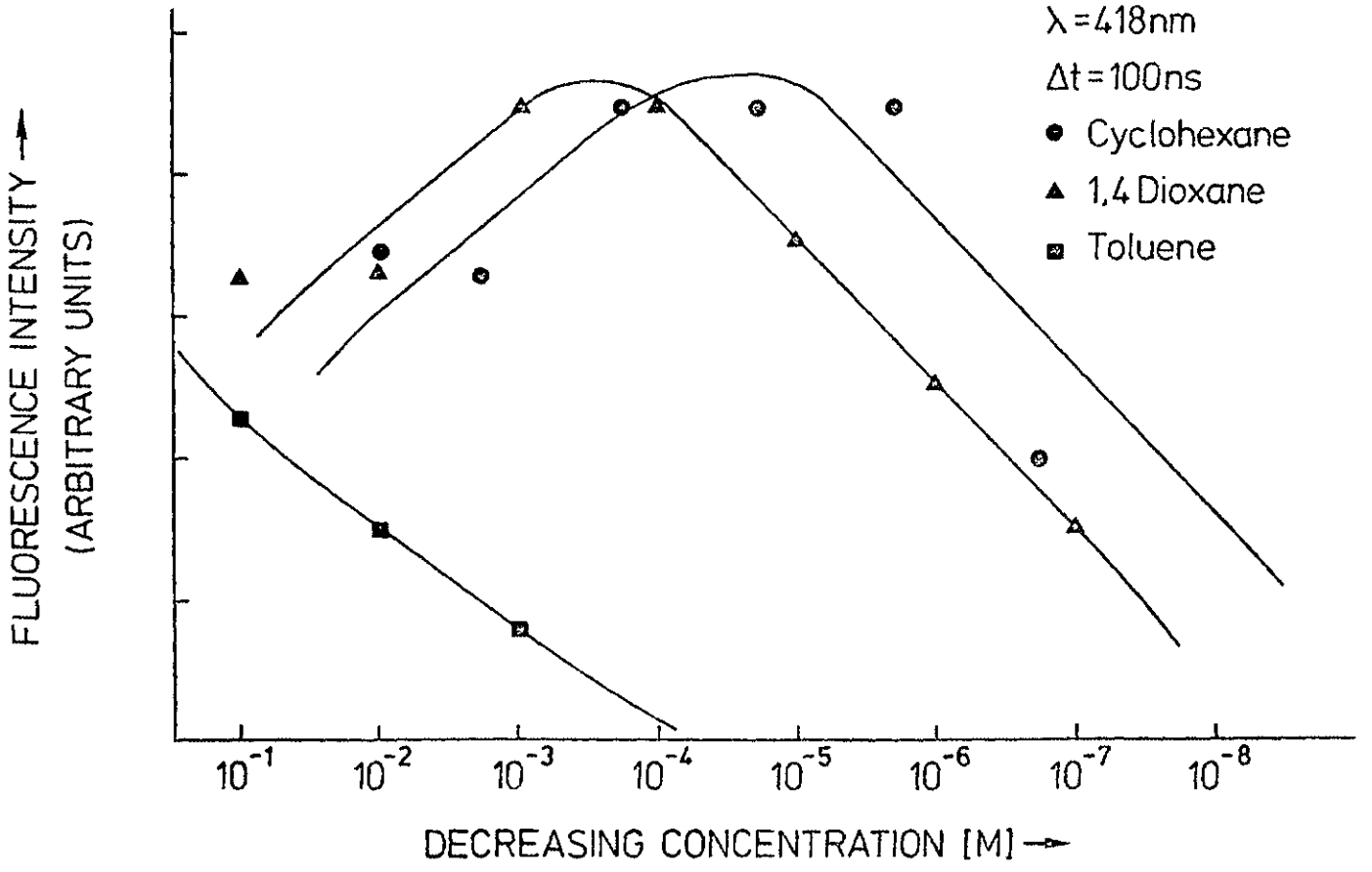

Figure 4-5. $S_1 \rightarrow S_0$ fluorescence component at 418 nm as a function of concentration for PPO in cyclohexane, 1,4 dioxane, and toluene

quenching effect is apparent, occurring in concentrations greater than 10^{-3} M.

Figure 4-4, shows the effect on excited state absorption of changing the solvent. The figure shows measurements made at 418 nm with a pump-probe delay, Δt, of 100 ns in solutions of cyclohexane, 1,4 dioxane and toluene. A concentration quenching effect is clearly evident in cyclohexane and 1,4 dioxane but not in toluene.

Figure 4-5 shows the effect of concentration on the fluorescence intensity for conditions prevailing in Figure 4-4. Our experimental set up allowed us to monitor only that component of the PPO $S_1 \longrightarrow S_0$ fluorescence that had the same wavelength as the probe beam. Figure 4-5 hence shows the effect of concentration on PPO fluorescence at 418 nm, this fluorescence corresponding to the signal shown in Figure 4-1 (b). There is good correlation between the results in Figure 4-4 and Figure 4-5 showing that the excited state absorption depends on the density of the S_1 states formed by the excimer pump. Hence as seen in Figure 4-5, the fluorescence also shows a concentration effect in cyclohexane as well as in 1,4 dioxane.

Experiments performed with solutions through which N_2 had been bubbled show an increase in excited state absorption of approximately 10% over the measurements performed with air-equilibrated solutions. The effect of bubbling O_2 through the solutions was to increase the

excited state absorption by approximately 15% compared to the air-equilibrated solutions.

Experiments For α-NPO (2,1 naphthyl, 5 phenylzole)

The α-NPO experiment was done without the boxcar averager. Figure 4-6 is a typical photograph showing how the record was taken. Figure 4-6 (a) shows the signal of dye probe incident on the sample cell with excimer radiation blocked off. This curve is the same as Figure 4-1 (a). We record the peak value from the scope, that is the incident light intensity I_o. In this photograph I_o is 1.7 V. Figure 4-6 (b) is the same as Figure 4-2 (c), which shows both the pump and probe radiation incident on the sample. The value of the probe reading from the scope is the emerging light intensity I. In this photograph I is 1.3 V. From these two values of I and I_o, we then calculate the absorption coefficient by using

$$U_d = - \ln(I/I_o).$$

Figure 4-7, shows the results of excited state absorption measurements on a solution of α-NPO in 1,4 dioxane at concentration 10^{-3} M, and dye probe delay time Δt = 70 ns. Because of the fluctuations of the dye laser probe, many measurements were taken and the plots are given with error bars. In this figure, two peaks are found at 390 nm and 455 nm respectively. These are the results of $T_1 \longrightarrow T_J$ and $T_1 \longrightarrow T_{J'}$ transition ($J' > J$, and $J \geq 2$).

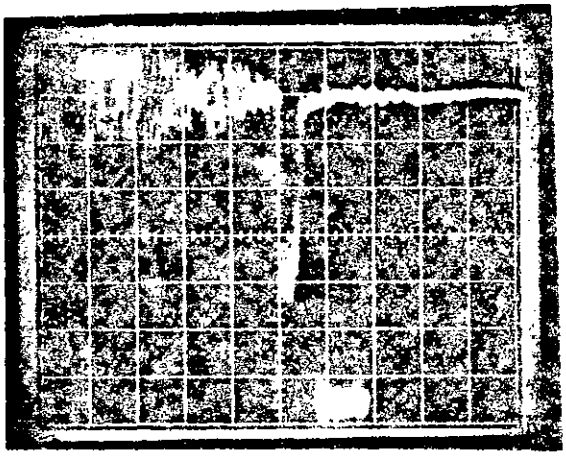

(A)

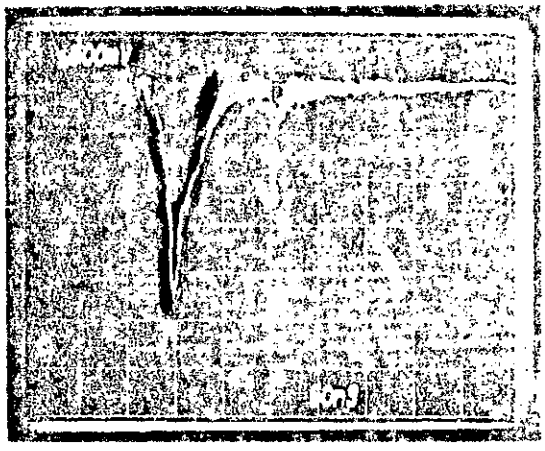

(B)

Figure 4-6. Sample results of α-NPO experiment from scope

Figure 4-8 shows the results for excited state absorption measurements on solutions of α -NPO in 1,4 dioxane at 460 nm and 492 nm with Δ t = 70 ns. A concentration quenching effect occurs in concentrations greater than 10^{-3} M which is about the same as that for PPO.

Figure 4-9, shows the excited state absorption versus dye-probe delay time (Δt) for α-NPO in 1,4 dioxane at concentration 10^{-3} M. This curve shows that the excited state absorption peaks around 60 ns.

These experiments were also performed on deaerated solutions by bubbling N_2, and show an increase in excited state absorption. When the solutions were saturated with O_2, a decreased excited state absorption was measured. These results are similar to the results obtained with PPO.

That the excited state absorption measured for both PPO and α-NPO is due to triplet-triplet absorption can be deduced from the above observations, which are summarized below:

(a) The singlet lifetime for PPO and α-NPO are in the range of 1-2 nano seconds [12]. In the experiment the excited state absorption increases with pump-probe delay time; in α-NPO peaking occurs around 60 nano second. While in PPO the excited state absorption occures around Δt = 100 nano seconds. This is much longer than the singlet lifetimes, which have lifetimes about two orders of

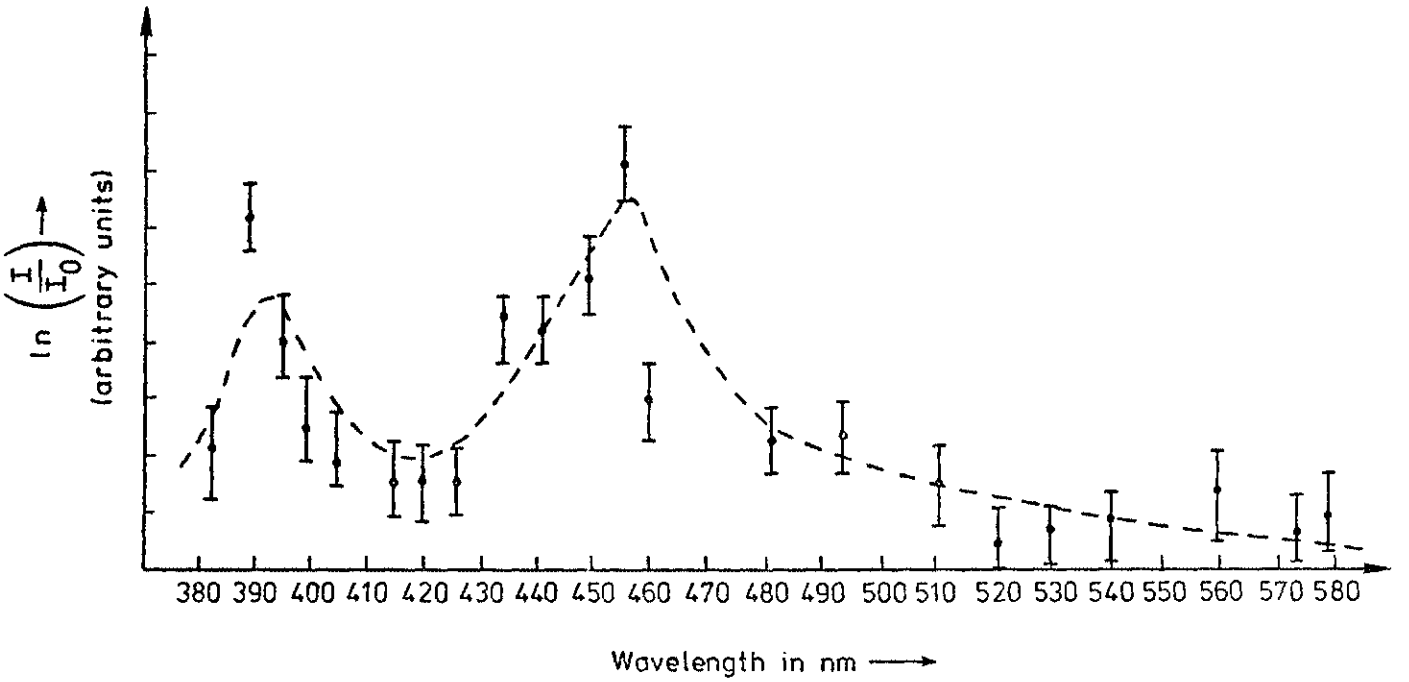

Figure 4-7. Excited state absorption measurements for α-NPO solution (10^{-3} M) in 1,4 dioxane

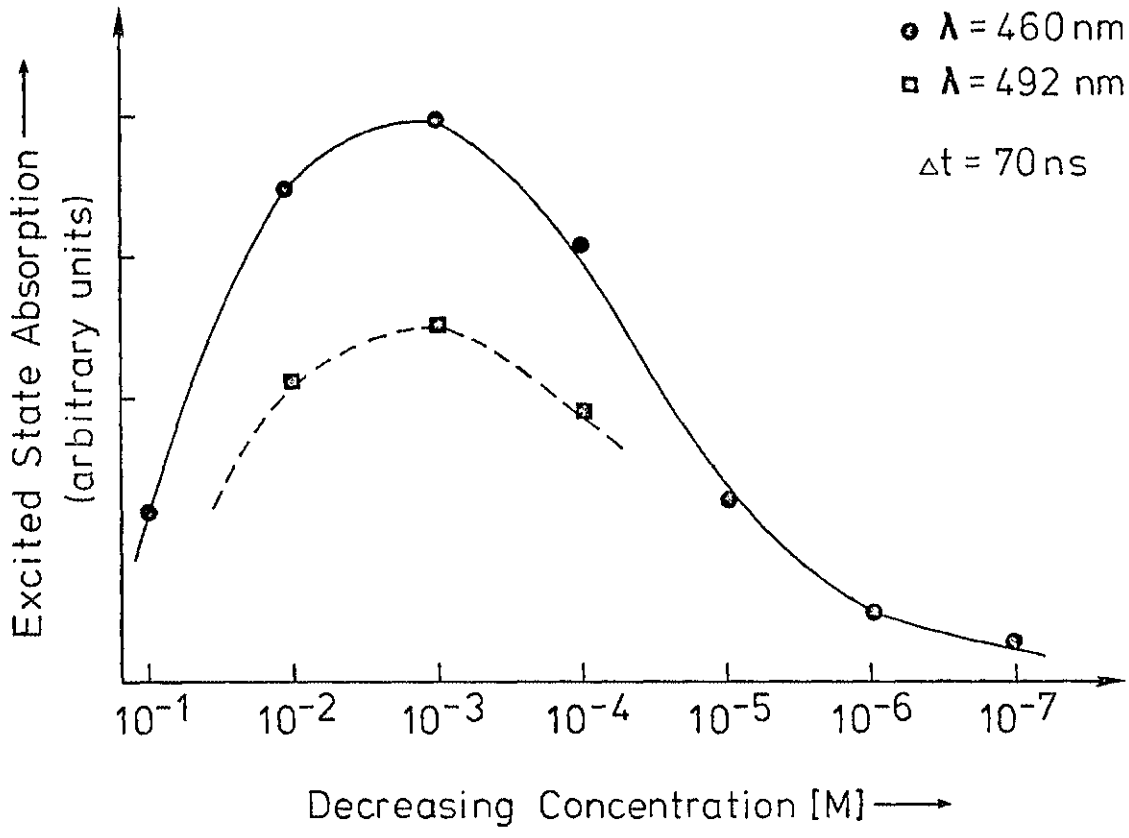

Figure 4-8. Excited state absorption for α-NPO in 1,4 dioxane as a function of concentration at 460, 492 nms with Δt = 70 ns

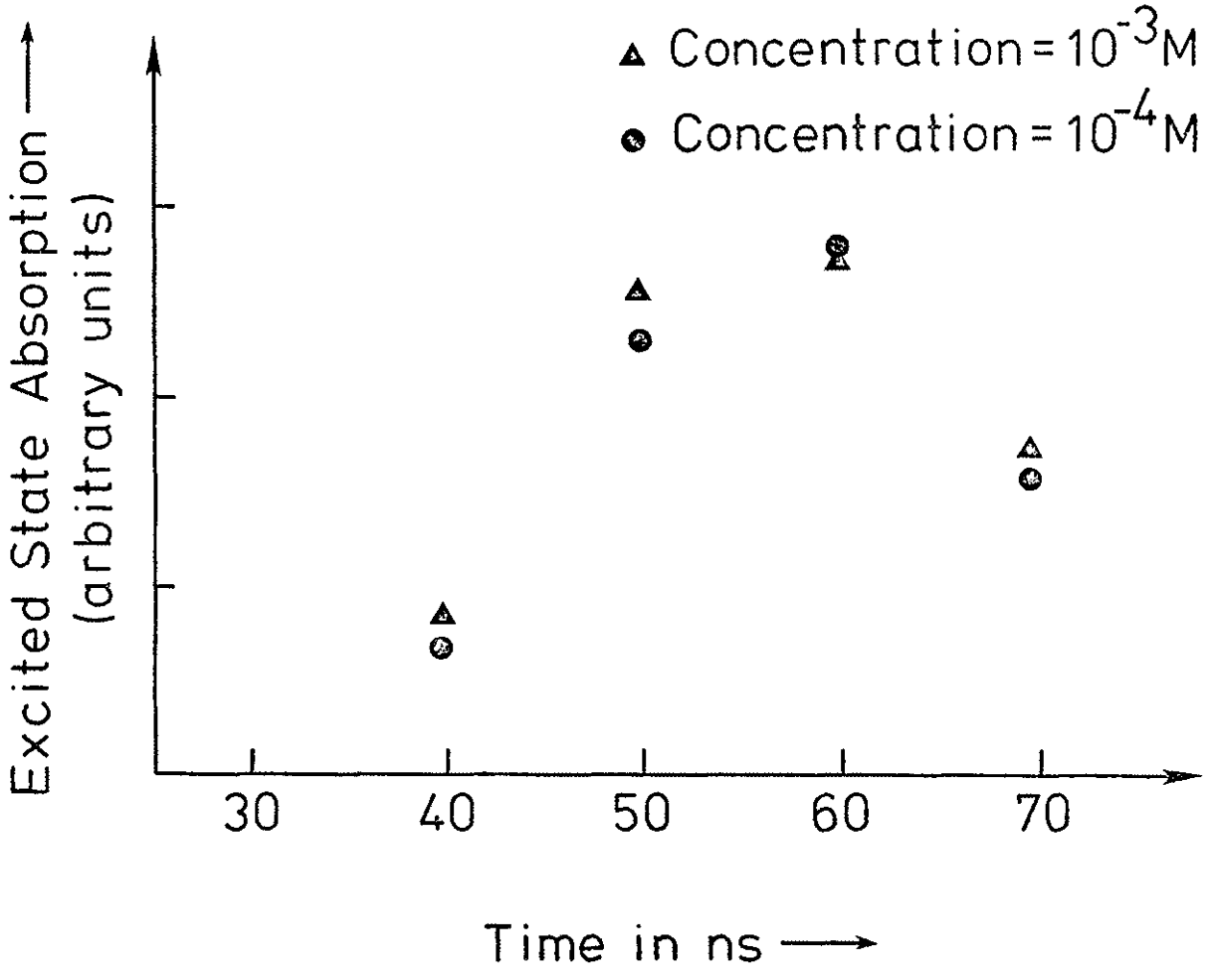

Figure 4-9. Excited state absorption for α-NPO in 1,4 dioxane (10^{-3} M, 10^{-4} M) as a function of probe delay time

magnitude shorter. Hence, the excited state absorption measured is not due to singlet-singlet transitions.

(b) The fact that quenching by molecular oxygen is much more associated with triplet-state than singlet state has been proved by Goldschmit et al.[14]. In PPO experiments, the excited state absorption for oxygen-saturated solutions decreased by approximately 25% compared to the deaerated solutions, with a similar result for α-NPO. The effect of bubbling O_2 through the solutions was to decrease the excited state absorption by approximately 30% compared to N_2 bubbled solutions. Such a large difference in oxygen effects would be unlikely for a singlet species.

(c) The excited state absorption dependence on concentration closely mimics that of PPO fluorescence, showing that the former is due to T_1 state populated via intersystem crossing from S_1.

(d) In these two experiments, the excited state absorption spectra observed are not due to any photoproducts, because it has been shown by Ackerman et al. [15] that such photoproduct formation is accelerated by the presence of O_2. The experiments with deoxygenated, air-equilibrated and oxygen-saturated solutions show that the excited state absorption measured decreased with increasing O_2 concentration.

Vapor Phases Experiments

For vapor phase experiments the procedure was similar to that for liquid experiments except that the sample cell had to be evacuated using the vacuum system mentioned in chapter III (see Figure 3-4). The appropriate gases were then introduced.

In this experiment, first we experimented on many molecules using various pressures and scanning all the possible probe wavelengths with t = 100 ns. Table IV-4 is the list of all molecules which were investigated. No excited state absorption was observed in any of them.

Table IV-5 gives the results for molecules with other mixtures. Still, no excited state absorption was observed, but some emission was found in certain molecules and photoproducts.

The reason for negative results with vapors could be either that the shortest probe wavelength was not energetic enough to probe $T_1 \rightarrow T_j$ transitions in the smaller molecules, or that there was very rapid radiationless relaxation of excited states in the vapor phase.

The next chapter gives the results of a numerical analysis performed. These are compared with the experimental results obtained.

Table IV-4 List of All Molecules Investigated in Vapor Phase

Molecules	Pressure (mbar)	Probe Wavelength (nm)
Benzene	1.1 -> 100	331 -> 480
Toluene	0.8 -> 1.3	322 -> 594
Pyrrole	1.1 -> 10.5(s)	327 -> 470
Mesitylene	1.0 -> 2.5(s)	330 -> 575
Ethylbenzene	1.0 -> 9.7(s)	327 -> 583
Bromobenzene	1.1 -> 5.1(s)	330 -> 588
Iodobenzene	1.1 -> 2.3(s)	354 -> 474
Pyridine	1.3 -> 19.8(s)	330 -> 577

(s) : saturated vapor pressure

Table IV-5 Molecules with Other Mixtures Which were Investigated

Molecule	Mixtures	Results
Pyrrole(5.4 mbar)	O_2 (10,35,100,780 mbar)	dissociation
Iodobenzene (0.5, 1 mbar)	n-pentane (530 mbar)	emission at 320->493(nm) photoproduct emission at 235.5(nm)
Mesitylene (0.5 mbar)	n-pentane(500mbar)	emission at 416->456(nm)
Pyrrole (0.5 mbar)	O_2 (10, 50,100 mbar) n-pentane(600 mbar)	emission at 327->389(nm)

Chapter V

NUMERICAL ANALYSIS

In this chapter we present results of a numerical analysis performed. Our approach was to develop the rate equations for the molecular excitation and dexcitation processes. Some of the rate constants were available from the literature. Those that were not were selected in such a way as to obtain the best fit possible between the numerical and experimental results. In this way, some rate constants, not measured previously, have been obtained.

Kinetic Rate Equations

Figure 2-1 shows a somewhat general schematic of lower energy levels of an organic molecule. The density of S_1 is governed by the equation V-1.

$$dS_1(t)/dt = \gamma(t) - (K_f + K_{isc} + K_{ic})S_1(t) - K_e S_1(t) S_0(t) \qquad (V\text{-}1)$$

or

$$dS_1(t)/dt = \gamma(t) - K_s S_1(t) - K_e S_1(t) S_0(t) \qquad (V\text{-}2)$$

where $K_s = K_f + K_{isc} + K_{ic}$ and $\gamma(t)$ is the pump term which depends on the excimer laser characteristics and the molecular concentration as well as the absorption cross-section. This latter term is described below. The

rate constant K_f refers to the radiative process of fluorescence

$$S_1 \xrightarrow{K_f} S_o + h\nu$$

from the excited singlet state (S_1) to ground state. The rate constant K_f has been found by Berlman for PPO to be $0.39 \times 10^9\ sec^{-1}$ and for α-NPO to be $0.36 \times 10^9\ sec^{-1}$ [12], which is much larger than the intersystem crossing rate K_{isc}, and the internal conversion K_{ic} which are usually several orders of magnitude smaller[33]. Hence, we have $K_s \simeq K_f$. The last term is due to excimer (D^*) formation via

$$S^* + S_o \xrightarrow{K_e} D^* .$$

K_e has been found by J. Yguerabide and M. Burton [32] to be $2.7 \times 10^9\ M^{-1}\text{-}sec^{-1}$ for PPO in cyclohexane. This equation describes the process by which molecules in the excited state (S_1) interact with those in the ground state forming the excited transient dimers, called excimers. The density of ground state molecules is time dependent; we can write

$$S_o(t) = S_o(0) - S_1(t) - T_1(t) .$$

The rate equation for triplet state T_1 is

$$dT_1(t)/dt = K_{isc} S_1(t) - K_t T_1(t) - K_{tt} [T_1(t)]^2 \qquad (V\text{-}3)$$

.

The first term of equation V-3, is the tripletformation rate from excited singlet S_1 state via

$$S_1 \xrightarrow{K_{isc}} T_1$$

where K_{isc} is the intersystem crossing rate. Birks [33] notes that this rate constant in aromatic hydrocarbons is about 10^6 sec^{-1} to 10^8 sec^{-1}.

The second term in equation V-3, is the triplet state quenching. Since oxygen is the most effective quencher of the triplet state [34-37], the rate constant K_t is

$$K_t = K_{qt}[O_2]$$

where K_{qt} is the second order rate constant quenching of the triplet state by O_2. Patterson et al [38] determined K_{qt} of some aromatic molecules, for example, Anthrone, Benzophenone, which are similar to PPO and α-NPO. They find a value of about 10^9 M^{-1}-sec^{-1} for these molecules in cyclohexane solution at 25° C. The oxygen concentration in cyclohexane solution at room temperature is 2.3×10^{-3} M [39].

The third term of the triplet rate equation is due to self-quenching of the triplets:

$$T_1 + T_1 \xrightarrow{K_{tt}} S_o + S_o .$$

Porter [40], estimates the rate constant K_{tt} to vary from 10^8 M^{-1}-sec^{-1} to 10^{10} M^{-1}-sec^{-1}. Wyrsch et al. [41] measured K_{tt} for 1:2-Benzanthracene in ethanol at room temperature to be about 10^{10} M^{-1}-sec^{-1}. Dupuy [42] also obtained a similar value of K_{tt}, for Chrysene in ethanol.

Pump Term

To derive an expression for the pumping term, we start by writing an expression for the change of the light beam intensity due to absorption by the absorbing medium

$$dI/dx = -I_o \exp(-n\sigma x)(n\sigma) \qquad \text{watts/cm}^3.$$

The average intensity absorbed per unit volume can be obtained by evaluating $\langle \Delta I \rangle_d = [1/d]\int_0^d [dI/dx]dx$.

$$\langle \Delta I \rangle_d = -[I_o/d]\,[1 - \exp(-n\sigma d)] \qquad \text{watts/cm}^3 \qquad \text{(V-5)}$$

where n represents some average density.

The intensity of the incident laser pulse depends on both time(t) and frequency(ν). Hence we write

$$I_o = I'_o(\nu) f(t) \qquad \text{watts/cm}^2$$

where I'_o has dimension of watts/cm^2 and f(t) is dimensionless. Substituting into equation V-5, we have

$$\langle \Delta I \rangle_d = -[f(t)/d] I'_o(\nu)[1-\exp(-n\sigma(\nu')d] \qquad \text{watts/cm}^3.$$

In order to account for the fact that absorption will only occur when the incident frequency(ν) is coincident with the absorption line at ν' for which the absorption cross-section is $\sigma(\nu')$, we write

$$\langle \Delta I \rangle_d = -\int_{\nu'} [I'_o(\nu)/d] f(t)[1-\exp(-n\,\sigma(\nu')d]\,\delta(\nu-\nu')d\nu'$$

watts/cm^3 (V-6).

This is the average power absorbed per unit volume, assuming that the incident laser is monochromatic (freq.ν).

Now we define an intensity spectral density $I''_o(\nu)$ (watts/cm^2 Hz) such that $dI'_o(\nu_o) = I''_o(\nu_o)d\nu$; $I''_o(\nu_o)$ is the intensity per unit frequency between ν_o and $\nu_o + d\nu$.

Then (V-6) yields

$$\langle I \rangle_d = (-f(t)/d) \int_{\nu} \int_{\nu'_o} I''_o(\nu) d\nu [1-\exp(-n\sigma(\nu)d] \delta(\nu-\nu') d\nu' \quad \text{watts/cm}^3 \qquad \text{(V-7)}.$$

Since the average pump photon energy is $h\nu$, equation (V-7) finally yields the pump term $\gamma(t)$:

$$\gamma(t) \simeq [I''_{oav}(\nu) f(t) \Delta\nu_{overlap} / h\nu_{av} d][1-\exp(-n\sigma_{av} d)] \quad \text{cm}^{-3}\text{sec}^{-1} \qquad \text{(V-8)}.$$

We modelled the temporal dependence of the experimental excimer laser pulse by the following equations

$$f(t) = A[1 - \exp(-rt)] \qquad 0 \leq t \leq t_1$$

$$f(t) = [1-\exp(-rt_1)]\exp[1-p(t-t_1)] \qquad t_1 \leq t < \infty$$

where constants A, r, p, and t_1 are found from experimental measurements to be;

$A = 1.01$ $\qquad r = 1.5 \times 10^8 \text{ sec}^{-1}$

$p = 5 \times 10^7 \text{ sec}^{-1}$ $\qquad t_1 = 20$ ns

$I''_{oav}(\nu)$ is measured experimentally as

$$I''_{oav}(\nu) = \frac{\text{Excimer energy}}{(\text{area of beam})(\text{pulse width})(\text{bandwidth})} .$$

The excimer energy was measured to be about 300 mj, using a pyrro electric detector. This had a pulsewidth (as measured on the scope) of 40 ns. The frequency bandwidth was measured to be between 2458 and 2508 Å.

$I''_{overlap}$ is the bandwidth of overlap between the pump and absorption band, and σ_{av} is the average absorption crossection over this bandwidth. The absorption bandwidth for PPO is from 230 nm to 350 nm and that for α-NPO is from 220 nm to 370 nm [12], both of which encompass the excimer bandwidth. Hence,

$\Delta\nu$ = excimer bandwidth.

Substituting all these constants into V-8, and using $\exp(-n\sigma d) = 10^{-\varepsilon M d}$, the pump term $\gamma(t)$ becomes

$$\gamma(t)=1.01K[1-\exp(-.15)t][1-10^{-\varepsilon M d}] \text{ cm}^{-3}\text{-sec}^{-1} \quad \text{for} \quad 0\leq t\leq 20$$

$$\gamma(t)=K[\exp(-.05t)][1-\exp(-.15t)][1-10^{-\varepsilon M d}] \text{ cm}^{-3}\text{-sec}^{-1} \quad \text{for} \quad 20\leq t< \infty$$

where $K=[I'_0(\nu)\Delta\nu/h\nu d] = 9.3 \times 10^{25} \text{ cm}^{-3}\text{-sec}^{-1}$.

This pump term was used in the computer program with the molecular extinction coefficient ε for PPO being 0.8×10^4 (lit/mole-cm) [43] and that for α-NPC being about 10^4 (lit/mole-cm) [12]. d is 1 cm in our experiment, M is the molar concentration (mole/lit).

Comparison of Numerical Result With Experimental Data

The relevant rate equations are

$$dS_1(t)/dt = \gamma(t)-K_s S_1(t)-K_e S_1(t)[S_0(0)-S_1(t)-T_1(t)] \qquad \text{(V-14)}$$

$$dT_1(t)/dt = K_{isc} S_1(t) -K_t T_1(t)-K_{tt} T_1^2(t) \qquad \text{(V-15)}.$$

These equations were written in the normalized form with following base values: time, 1 ns, concentration, 10^{17} cm^{-3}. They were solved numerically, using Euler's Modified Method of the predictor-corrector type (appendix A). A FORTRAN program (see appendix B) was written and executed on a VAX 11/780 computer.

Table V-1 is a list of the constants used in the numerical analysis. Some constants were available from the literature and were used, while others had not been measured previously. These were found by varying them, in such a way that the best possible fit to experimental results was obtained. Figure 5-1 shows the experimentally obtained fluorescence intensity versus time, together with the numerical results which were obtained by substituting the constants in table V-1 into the rate equations. The fitting was done by normalizing the peak numerical value to the experimental one. Figure 5-2 shows the experimentally and numerically obtained time dependence of excited state absorption for PPO in 1,4 dioxane at a concentration of 10^{-3} M. The numerical result shows that PPO triplet peaks at 104 ns after irradiation, which also proved that the triplet lifetime was about two orders of magnitude longer than that of the singlet. The vertical error bar shows the experimental maximum and minimum values, this was the result of the fluctuation of the excimer laser, and the horizontal error bar shows the estimated error in the measurement of Δ t. This error was

about ± 5 ns. Figure 5-3 and Figure 5-4 show the time dependence of excited state absorption for α-NPO in 1,4 dioxane at concentrations 10^{-3} M and 10^{-4} M respectively. The excited state absorption is larger at 10^{-3} M than 10^{-4} M, which is as expected, since the peak absorption occurs at concentration 10^{-3} M (Figure 4-8). Figure 5-5 and 5-6 show the numerical and experimental results of fluorescence and triplet density versus concentration for PPO in 1,4 dioxane, which also show the excimer formation at higher concentration. The experimental results show that this concentration effect appears for PPO in 1,4 dioxane and cyclohexane but not in toluene. This is explained by the fact that excimer formation occurs much less readily in aromatic solvents than in nonaromatics [45]. If we use excimer formation rate, $K_e = 0$, in our numerical equations the concentration effect will not appear. This is presently being attempted by another graduate student. However there are complications that arise because of absorption of the 248 nm radiation by toluene itself. Figure 5-7, shows the numerical and experimental results for α-NPO in 1,4 dioxane for excited state absorption versus concentration. Here we find the concentration effect appearing at around 10^{-3} M. Since α-NPO has a low solubility in cyclohexane, we were not able to conduct similar experiments for this solvent.

In this numerical model we considered only the excitation of S_1 by the KrF pump. But we know that S_j, $j>1$,

are formed when the molecules are pumped. The rate equations given above, do not take this into consideration. However, since the internal conversion $S_j \rightarrow S_1$ occurs on a time scale of picoseconds, the results obtained are fairly accurate. Another point that the numerical model does not take into consideration is the probe pulse. In principle, T_1 is perturbed somewhat by the probe laser. However, the energy of the probe dye is much smaller than that of the KrF pump. Hence the probe pulse can be ignored in the rate equation formulation. On the whole, this model is valuable and it shows very good agreement with our experimental results.

Table V-1 Rate Constants for PPO and α-NPO

	α-NPO	PPO
K_s	[45] 0.36×10^{9} sec^{-1}	0.39×10^{9} sec^{-1} [45]
K_{isc}	[*] 3.3×10^{6} sec^{-1}	2.9×10^{6} sec^{-1} [*]
K_e	[*] 7.5×10^{-12} $cm^3\text{-}sec^{-1}$	4.5×10^{-12} $cm^3\text{-}sec^{-1}$ [32]
K_{qt}	[*] 1.8×10^{-12} $cm^3\text{-}sec^{-1}$	0.12×10^{-12} $cm^3\text{-}sec^{-1}$ [*]
K_t **	[*] 2.5×10^{6} sec^{-1}	1.6×10^{5} sec^{-1} [*]
K_{tt}	[*] 6.8×10^{-11} $cm^3\text{-}sec^{-1}$	3.2×10^{-12} $cm^3\text{-}sec^{-1}$ [*]
ε	[12] 10^{4} lit/(mole-cm)	0.8×10^{4} lit/(mole-cm) [43]

* : These values are obtained from best fit of numerical and experimental results.

**: $K_t = K_{qt} [O_2]$, where $[O_2]$ is density of dissolved oxygen in air-equilibrated solutions.

$[O_2] = 2.3 \times 10^{-3}$ M [39]

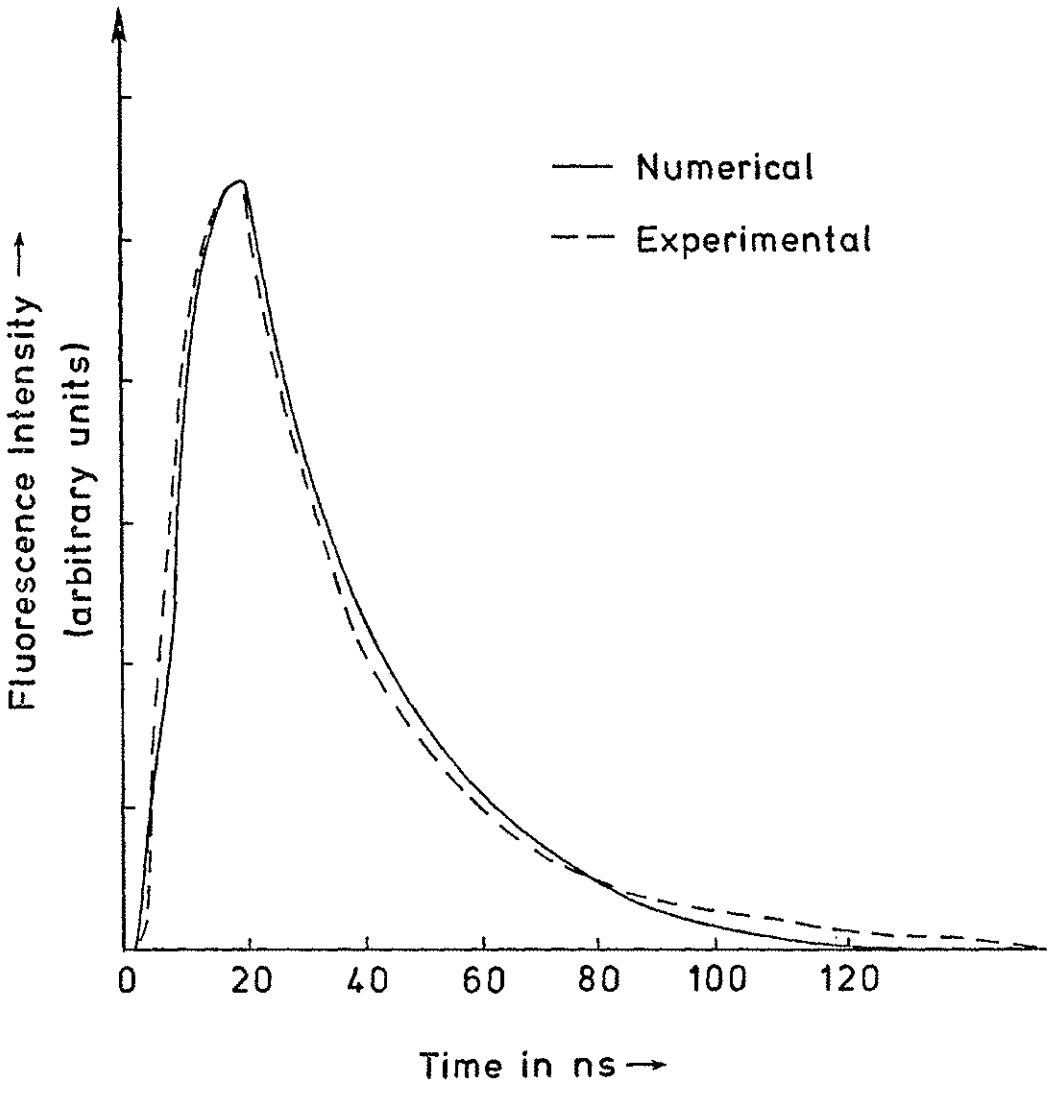

Figure 5-1. Experimental and computed fluorescence intensity as a function of time

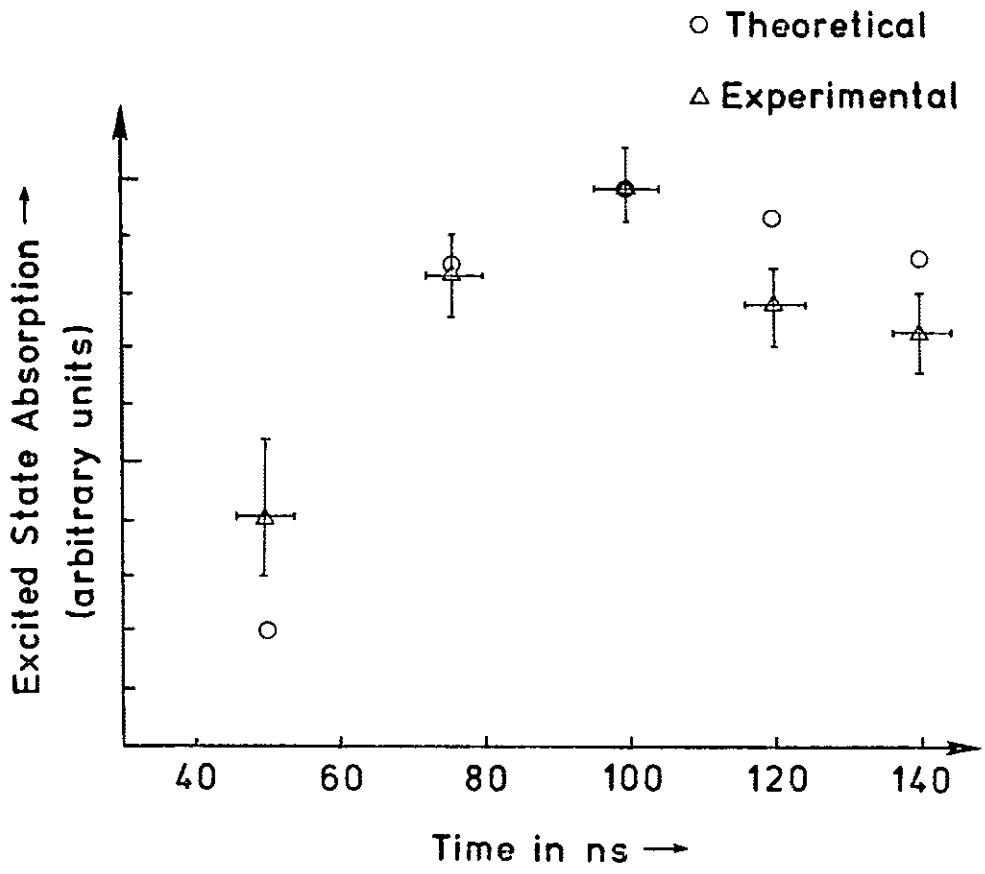

Figure 5-2. Comparison of experimental and computed excited state absorption as a function of time for PPO solution (10^{-3}M) in 1,4 dioxane

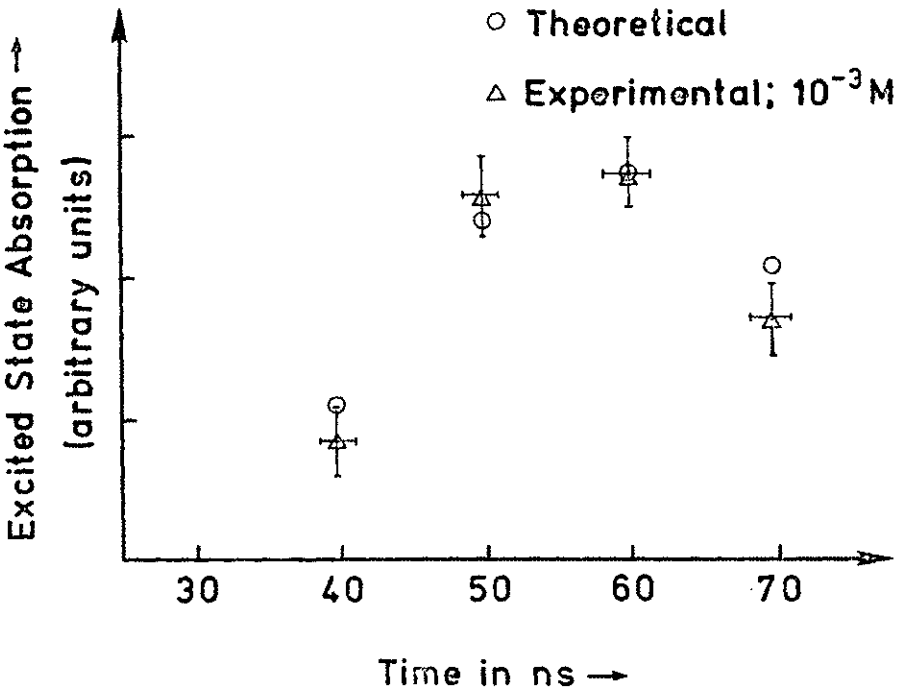

Figure 5-3. Comparison of experimental and computed excited state absorption as a function of time for α-NPO solution (10^{-3} M) in 1,4 dioxane

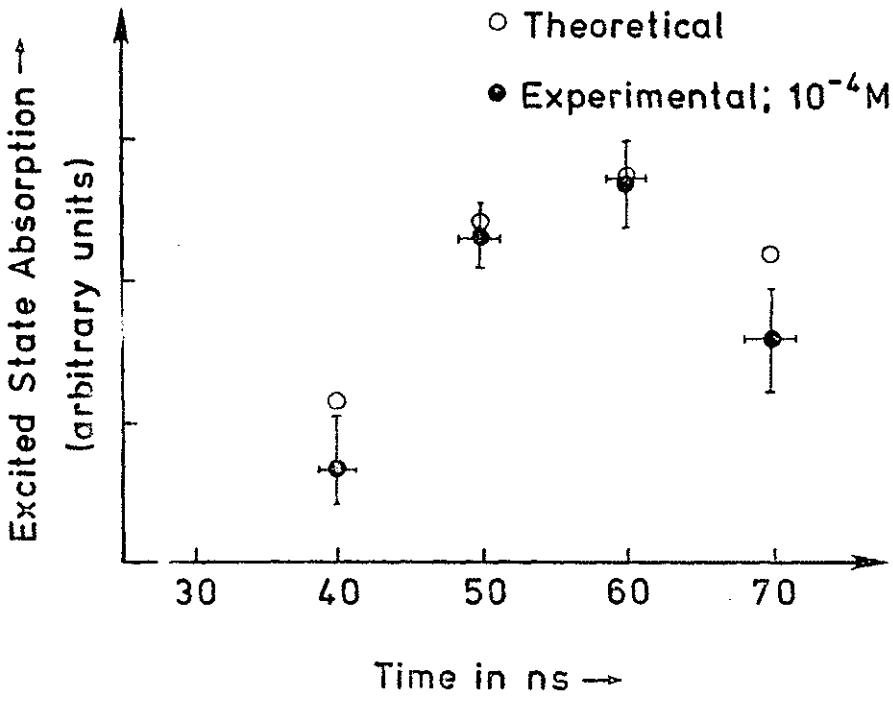

Figure 5-4. Comparison of experimental and computed excited state absorption as a function of time for α-NPO solution (10^{-4} M) in 1,4 dioxane

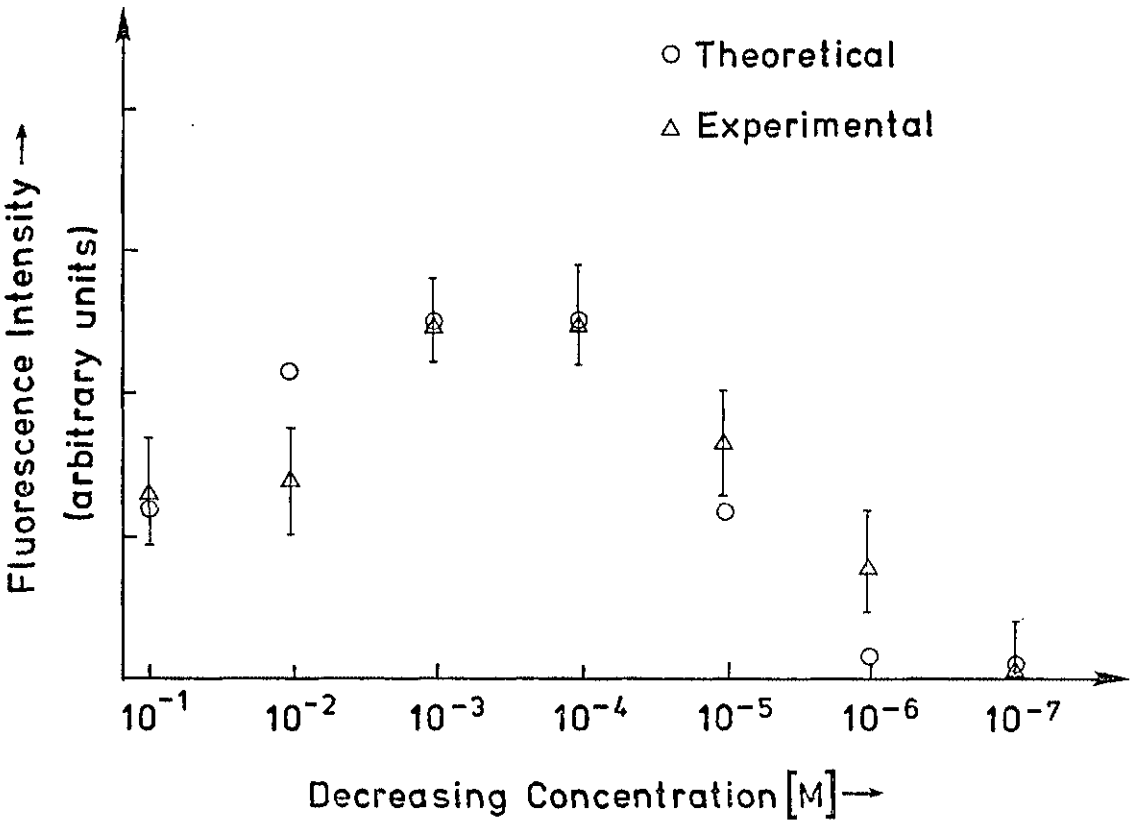

Figure 5-5. Comparison of experimental and computed fluorescence intensity as a function of concentration for PPO in 1,4 dioxane at λ = 418 nm and Δ t = 100 ns

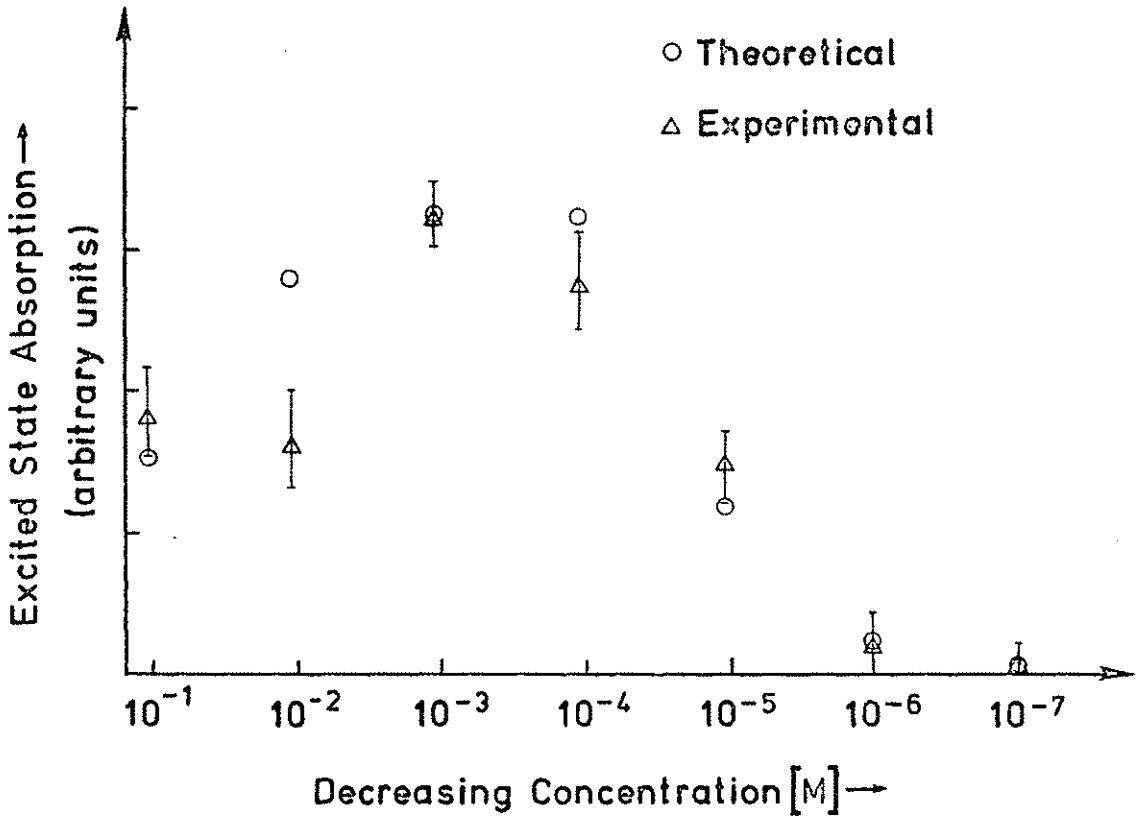

Figure 5-6. Comparison of experimental and computed excited state absorption as a function of concentration for PPO in 1,4 dioxane at λ = 418 nm and Δ t = 100 ns

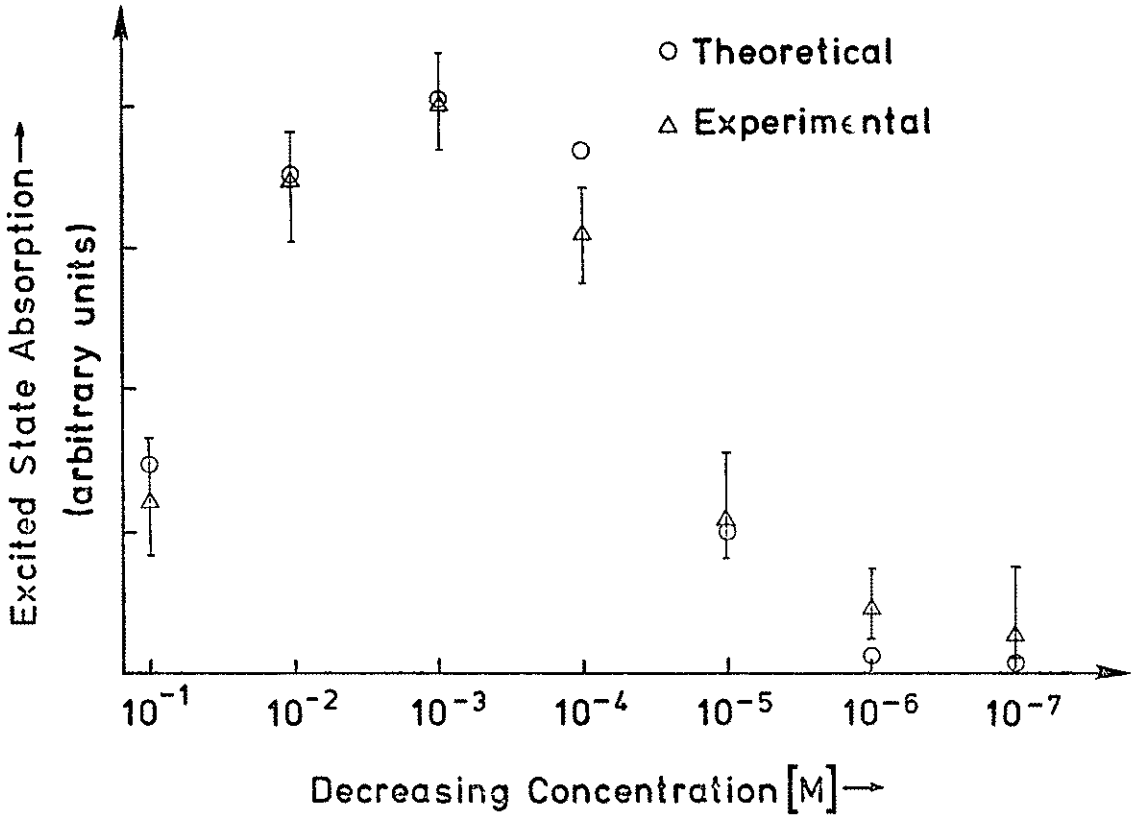

Figure 5-7. Comparison of experimental and computed excited state absorption as a function of concentration for α-NPO in 1.4 dioxane at λ = 460 nm and Δt = 70 ns

Chapter VI

CONCLUSION

In the experiments described in this thesis, we investigated excited state absorption by using a laser pump and probe technique. The excited state absorption of PPO and α-NPO was proved to be due to triplet-triplet absorption.

The experimental results were explained by numerical analysis of the relevant rate equations. This analysis provided a good fit of the experimental dependence of the triplet density on time and concentration as well, it resulted in the expected behavior of the triplet and singlet densities when the rate constants were changed. For example, an increase in the intersystem crossing rate K_{isc} resulted, in general, in an increase of the triplet density and a decrease in the singlet density. Similarly an increase in K_f, the rate constant for fluorescent decay ($K_s = K_f + K_{isc} + K_{ic} - K_f$), resulted in a decrease in S_1 and T_1 densities. This is to be expected because an increased K_s implies a faster depletion rate for S_1, all other conditions being the same.

The rate constants for triplet quenching by oxygen K_t and triplet-triplet self-quenching K_{tt}, are the decay paths for the triplet state T_1, and control its peaking

time (t_o). If K_t and K_{tt} are decreased then t_o increases. These results are quite reasonable. In the experiment, we measured t_o to be about 110 ns for PPO and 60 ns for α-NPO solutions. By fitting these results, we obtained the rate constants K_t and K_{tt} for PPO and -NPO. Because the α-NPO molecule is larger than PPO molecule, it has a greater spinorbit coupling [50]. The greater the spinorbit coupling, the larger the allowedness of singlet<—>triplet transition. Hence one would expect values of K_t and K_{tt} for α-NPO which are larger than those for PPO. From the point of view that a larger molecule has greater collision probability, we also expected that α-NPO would have a larger value of self-quenching rate (K_e) than PPO. This was indeed verified by the results.

In the vapor phase experiments, we did not find any excited state absorption. A reason might be that the triplet lifetimes for the molecules investigated are too short; some organic molecules with similar electronic structures as the molecules we used have a very short triplet collision-free lifetime of about 40 ns [51-53]. Owing to the molecular collisions in gaseous form, the triplet state could have an effective lifetime which might be even shorter (<10 ns). Such states would not be detected in our experiment, which had a time resolution of about 10 to 15 ns. Another possible reason might be that

the shortest probe wavelength in our experiment (340 nm) wasnot short enough to cause a $T_1 - T_j$ ($j \geq 2$) transition.

In terms of future work that might be done, one may suggest an improved time resolution. The time resolution might be improved by pulse compression techniques using saturable dye absorbers. An order of magnitude improvement might then arise. A more expensive alternative, which however would provide much better time resolution, would be to use two doubled dye lasers pumped by the same laser. Picosecond resolution could be obtained by using, for example, a mode locked, synchronously pumped, Nd-Yag or Ar ion laser as the driver laser. Further experimentation with buffer gases might also be useful.

A great improvement in the experiment would be obtained if the driver laser (the excimer in our case) did not fluctuate as much as it did during our experiments. This would enable weaker absorptive transitions to be detected. Along these lines, the detection sensitivity could be considerably enhanced if the data gathering and processing aspects of the experimental set up were improved, for example by the addition of a boxcar averager.

REFERENCES

[1] A. N. Dharamsi and Shawpin Jong, "Excited State Absorption Measurement in 2,5 Diphenyloxazole (PPO) Solutions," SPIE(Society of Photo-Optical Instrumentation Engineers), Quebec International Symposium, 1986.

[2] I. B. Berlman, "Handbook of Fluorescence Spectra of Aromatic Molecules," Academic Press, New York, pp. 147-157, 1965.

[3] J. T. Verdeyen, "Laser Electronics," Prentice Hall, pp. 264-268, 1981.

[4] H. Labhart and W. Heizelman, "Organic Molecular Photophysics," vol. 1. Editor: J. B. Birks, Wiley-Interscience, New York, pp. 297-348, 1973.

[5] A. N. Dharamsi and J. Tulip, "Contact Charge Transfer Lasers," J. Appl. Phys., vol. 52, pp. 4418-4421, 1981.

[6] R. S. Mulliken and W. B. Person, "Molecular Complexes," New York: Wiley-Interscience, 1969.

[7] S. Okajima and E. C. Lim, "Excitation Energy and Isotope Dependence of Exciplex Formation in The Vapor Phase," Chem. Phys. Letters., vol. 70, pp.283-286, 1980.

[8] G. Porter and M. W. Winsor, "The Triplet State In Fluid Media," Proc. Roy. Soc. London. A. vol. 245, pp. 238-258, 1958.

[9] T. Nakayama, Y. Yabuuahi, Y. Kajiwara, "Time-Dependent $T' \leftarrow T_1$ absorption spectra of 4'-Benzole-2,4,6-triisopropyl Benzophenone in Solutions," Chem. Phys. Letters., vol. 115, pp. 55-59, 1985.

[10] J. B. Birks, "Organic Scintillators and Liquid Scintillation Counting," Editors: D. L. Horrocks and C. T. Peng, Academic Press, New York, pp. 2-23, 1971.

[11] I. B. Berlman, "Efficiency of Energy Transfer in a Solution of PPO in Xylene," J. Chem. Phys., vol. 33, pp. 1124-1127, 1960.

[12] H. Lami and G. Laustriat, "Excimer Formation with Polar Molecules Oxazole and Oxadiazole Derivatives," J. Chem. Phys., vol. 48, pp. 1832-1840, 1968.

[13] Essam Nasser, "Fundamentals of Gaseous Ionization and Plasma Electronics," John Wiley & Sons Inc., pp. 85-93, 1971.

[14] C. R. Goldschmidt, R. Potashnik, and M. Ottolenghi, "Intersystem Crossing in the Charge-Transfer Quenching of Molecular Fluorescence," J. Phys. Chem., vol. 75, pp. 1025-1031, 1971.

[15] M. E. Ackerman, G. H. Daub, F. N. Hayes and H. A. Mackay, "Organic Scintillators and Liquid Scintillation Counting," Editors: D.L. Horrocks and C. T. Peng, Academic Press, New York, PP. 315-326, 1971.

[16] B. B. Snavely, "Organic Molecular Photophysics," vol. 1, Editor:J. B. Birks, Wiley-Interscience, New York, pp. 239-296, 1973.

[17] S. P. Mcglynn, T. Azumi, M. Kinoshita, "Molecular Spectroscopy of the Triplet State," Prentice Hall Inc., pp. 5-9, 1969.

[18] G. N. Lewis and M. Kasha, "Phosphorescence and Triplet State," J. Am. Chem. Soc., vol. 66, pp. 2100-2116, 1944.

[19] G. Porter, F. R. S. and F. Wilkinson, "Energy Transfer From The Triplet State," Proc. Roy. Soc. London, vol. 264, pp. 1-18, 1961.

[20] G. Porter, "Flash Photolysis and Spectroscopy A New Method For The Study of Free Radical Reactions," Proc. Roy. Soc. London, A. vol. 200, pp. 284-300, 1950.

[21] J. R. Novark and M. W. Windsor, "Laser Photolysis and Spectroscopy: A New Technique for the Study of Rapid Reactions in the Nanosecond Time Range," Proc. Roy. Soc. London, vol. 308, pp. 95-110, 1968.

[22] Kumao Hamanoue et.al., "Excimer Formation of Neat Benzene Derivatives Studied by Picosecond Spectroscopy," Chem. Phys. Letters., vol. 82, pp. 55-62, 1981.

[23] A. N. Dharamsi, "Theoretical Potential Energy Curves for Triplet H_2O-O_2Contact Charge Transfer Complexes," Chem. Phys. Letts. vol. 108, pp. 166-168, 1984.

[24] A. N. Dharamsi and J. Tulip, "A CNDO/S Investigation of Contact Charge Transfer Complexes of Some Organic Molecules with O_2 ," Chem. Phys. Letters., vol. 71, pp. 224-227, 1980.

[25] A. N. Dharamsi and J. Tulip, "Comment on A CNDO/S Investigation of Contact Charge Transfer Complexes," ",Chem. Phys. Letters. vol. 75, pp. 406-407, 1980.

[26] C. C. Lo and Leskovar, "Evaluation of Hamamatsu Photomultiplier," Rev. Sci. Instrum., vol. 55 pp. 1100-1103, 1984.

[27] K. Morokuma, "Why Do Molecules Interact ? The Origin of Electron Donor-Acceptor Complexes, Hydrogen Bonding and Proton Affinity," Account's of Chem. Res., vol. 10, pp. 294-300, 1977.

[28] R. S. Mulliken, "Structures of Complexes Formed by Halogen Molecules with Aromatic and with Oxygenated Solvents," J. Am. Chem. Soc., vol. 72, pp. 600-608, 1950.

[29] R. S. Mulliken, "Molecular Compounds and their Spectra II," J. Am. Chem. Soc., vol. 64, pp. 811-824, 1952.

[30] R. S. Mulliken, "Lewis Acids and Bases and Molecular Complexes," J. Chem. Phys. vol. 19, pp.514-515, 1951.

[31] R. S. Mulliken,"The Interaction of Electron Donor and Acceptor Molecules," Symp. Mol. Phys., 1953.

[32] Juan Yguerabide and Milton Burton, "Luminescence Decay Times: Concentration Effect," J. Chem. Phys., vol. 37, pp. 1757-1774, 1962.

[33] J. B. Birks, "Organic Molecular Photophysics," John Wiley & Sons Inc., vol. 2, pp. 140-142, 1975.

[34] K. Kawaoka, A. U. Khan and D. R. Kerns, "Role of Singlet Excited State of Molecular Oxygen in the Quenching of Organic Triplet States," J. Chem. Phys., vol. 46, pp. 1842-1853, 1967.

[35] D. R. Kearns, A. J. Stone, "Excited-State Intermolecular Interactions Involving Paramagnetic Molecules: Effect of Spin-Spin and Spin-Orbit Interactions on the Quenching of Triplets," J. Chem. Phys., Vol. 55, pp. 3383-3389, 1967.

[36] E. I. Hormats and F. C. Untereitner, "Measurement of the Diffusion of Oxygen in Polymers by Phosphorescent Quenching," J. Phys. Chem., vol. 69, pp. 3677-3681, 1965.

[37] S. Siegel and H. S. Judeikis, "Relative Interaction Radii for Quenching of Triplet-State Molecules," J. Chem. Phys., vol.48, pp. 1613-1619, 1968.

[38] L. K. Patterson, G. Porter And M. Topp, "Oxygen Quenching of Singlet and Triplet State," Chem. Phys. Letters., vol. 7, pp. 612-614, 1970.

[39] C. S. Parmenter and J. D. Rau, "Fluorescence Quenching in Aromatic Hydrocarbons by Oxygen," J. Chem. Phys., vol. 51, pp. 2242-2246, 1969.

[40] G. Porter and M. R. Wright, "Intermolecular and Intermolecular Energy Conversion Involving Change of Multiplicity," Disc. Faraday. Soc., vol. 27, pp. 18-27, 1959.

[41] D. Wyrsch and H. Labhart, "Investigation on the Triplet Decay Mechanisms of 1,2-Benzanthracene in Solution," Chem. Phys. Letters., vol. 12, pp. 373-381, 1971.

[42] F. Dupuy, "The Role of Molecular Association in the Temperature Induced Increase of the Delayed Fluorescence of Vitreous Solutions of Aromatic Compounds," Chem. Phys. Letters., vol. 13, pp. 537-540, 1972.

[43] G. Porter, F. R. S. and M. R. Topp, "Nanosecond Flash Photophysis," Proc. Roy. Soc. London, vol. 315, pp. 163-184, 1970.

[44] F. Wilkinson, "Organic Molecular Photophysics," Vol. 2, Editor: J.B. Birks, Wiley-Interscience, New York, pp. 139-145, 1975.

[45] I. B. Berlman, "Transient Dimer Formation by 2,5-Diphenyloxazole," J. Chem. Phys., vol. 34, pp. 1083-1084, 1961.

[46] A. D. Osborne and G. Porter, F. R. S., "Diffusion Studies in Viscous Media," Proc. Roy. Soc. London, vol. 279, pp. 9-16, 1965.

[47] J. W. Eilpern, G. Porter, F. R. S. and L. J. Stief, "Decay of the Triplet State," Proc. Roy. Soc. London, vol. 277, pp. 437-447, 1964.

[48] J. P. Simons, "Photochemistry and Spectroscopy," John Wiley & Sons Ltd., pp. 158-162, 1971.

[49] A. D. Boardman, "Physics Programs," John Wiley & Sons Ltd., pp. 158-162, 1971.

[50] S. P. Mcglynn, T. Azumi, M. Kinoshita, "Molecular Spectroscopy of The Triplet State," Prentice Hall Inc., pp. 183-189, 1969.

[51] M. A. Duncan, T. G. Dietz, M. G. Liveman and R. E. Smalley, "Photoionization Measurement of the Triplet Lifetime of Benzene," J. Phys. Chem., vol. 85, pp. 7-9, 1981.

[52] T. G. Dietz, M. A. Duncan and R. E. Smalley, "Time Evolution Studies of Triplet Toluene by Two-Color Photoionization," J. Chem. Phys.,pp. 1227-1232, 1982.

[53] T. G. Dietz, M. A. Duncan, A. C. Pulu and R. E. Smalley, "Pyrazine and Pyrimidine Triplet Decay in a Supersonic Beam," J. Phys. Chem vol. 86, pp. 4026-4029, 1982.

[54] R. S. Mulliken and W. B. Person, "Molecular Complexes," New York: Wiley-Interscience, pp. 210-216, 1969.

APPENDIX

A. Numerical Method

B. Flow-Chart and FORTRAN Program for RATE.F

Appendix A

NUMERICAL METHOD [49]

The numerical method chosen to solve the rate equations is Euler's Modified Method, which is a self-starting method of the predictor-corrector type, having greater accuracy than Euler's method. It is also known as Quinn's method and often referred to as Euler's improved method.

We consider the singlet and triplet rate equations:

$$dS_1(t)/dt = S'(t) = \gamma(t) - K_s S_1(t) - K_e [S_o(0) - S_1(t) - T_1(t)] \quad A1$$

$$dT_1(t)/dt = T'(t) = K_{isc} S_1(t) - K_t T_1(t) - K_{tt} T_1(t) \quad A2$$

for the initial condition at $t = 0$ we have $S(0) = 0$ and $T(t) = 0$. Hence $S'(t)$ and $T'(t)$ at $t = 0$ are known.

Given $S'(t)$ and $T'(t)$ we can estimate the value at $t + \Delta t$ by

$$S(t+\Delta t) = S(t) + S'(t)\ (\Delta t) \quad A3$$

$$T(t+\Delta t) = T(t) + T'(t)\ (\Delta t). \quad A4$$

These two equations A3, A4, are known as Euler's forward-integration equations. By comparing these two equations with Taylor's-series for Y_i expend about X_i,

with the Lagragian form of the remainder,

$$Y_{i+1} = Y_i + Y'_i\ h + Y''_i(e)h\ /\ 2\ . \qquad A5$$

The last term of equation A-5 is the truncation-error in Euler's Method. Because we are neglecting terms containing (Δt) and subsequent higher power of (Δt), the per-step error is of order $(\Delta t)^2$ for Euler's Method.

In Euler's Modified Method, every step in Euler's Method is divided by two. The first step gives the predictor, obtained in the same way as in Euler's Method but taking the interval to be $\Delta t/2$. Hence equations A6 and A7 are obtained for the predictor:

$$S(t+\Delta t/2) = S(t) + S'(t)(\Delta t/2) \qquad A6$$

$$T(t+\Delta t/2) = T(t) + T'(t)(\Delta t/2). \qquad A7$$

The equations for the corrector part are

$$S(t+\Delta t) = S(t) + S'(t+\Delta t/2)(\Delta t) \qquad A8$$

$$T(t+\Delta t) = T(t) + T'(t+\Delta t/2)(\Delta t). \qquad A9$$

Where $S'(t+\Delta t/2)$ and $T'(t+\Delta t/2)$ can be obtained from equations A1 and A2. If substitute A6 and A7 into A8 and

A9, and compare with the Taylors-series for Y expanded about X_i, we obtain

$$Y_{i+1} = Y_i + Y'_i\, h + \frac{Y''_i h^2}{2!} + \frac{Y'''(e) h^3}{3!} \quad , X_i < e < X_{i+1} \quad . \qquad A10$$

It can be seen that the per-step truncation error of the corrector equation is of order $(\Delta t)^3$.

In the computer program, we let $\Delta t = 0.01$, so an estimate of the truncation error in computing $S(t+\Delta t)$ and $T(t+\Delta t)$ is $(\Delta t)^3 = 10^{-6}$.

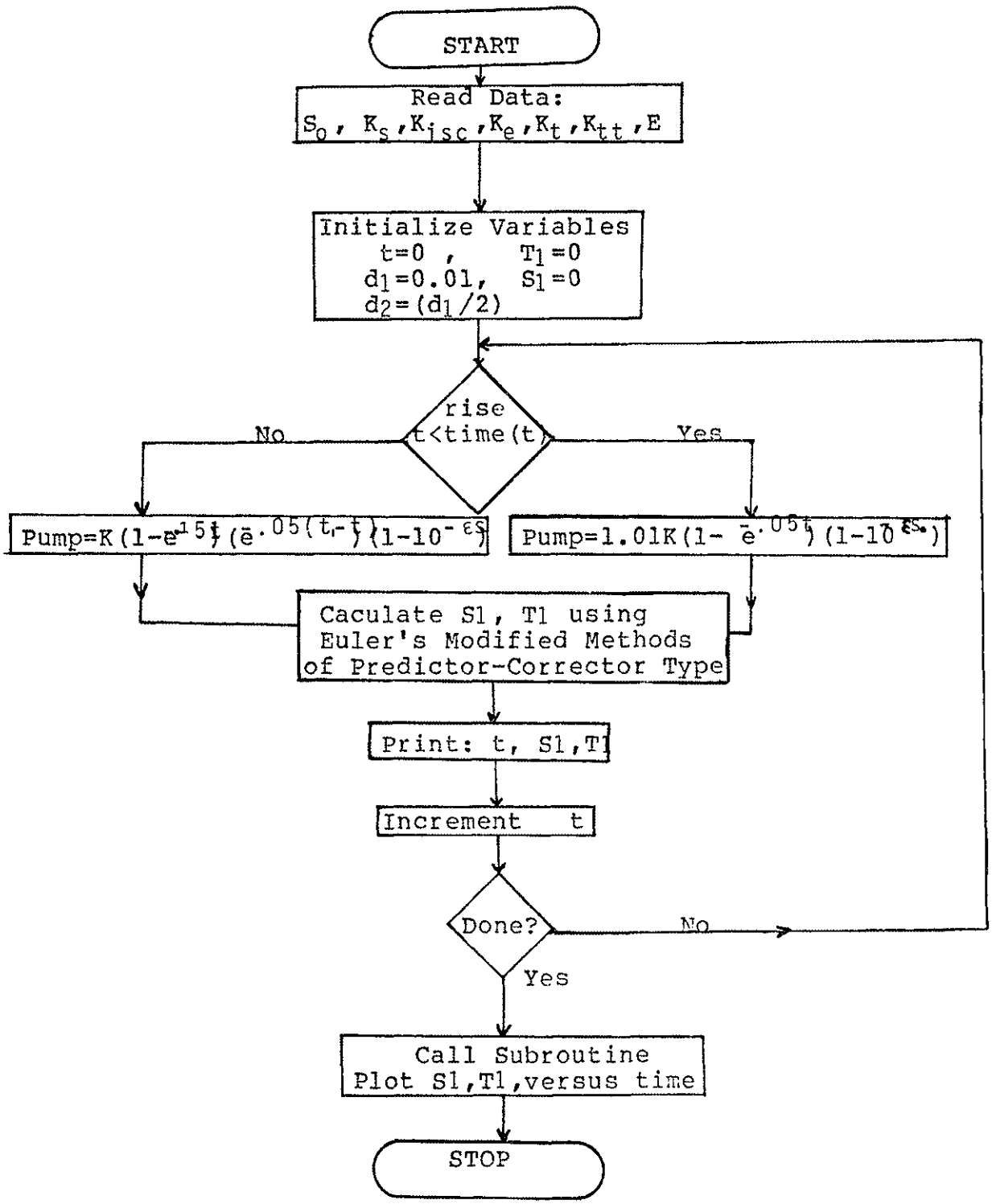

Figure A-1, Flow-Chart of Computer Program Solving the Rate Equation.

```
c       PROGRAM NAME IS  RATE.F
c       UES FOR CACULATE THE RATE EQUATION OF SINGLET AND TRIPLET STATE
c       SUBROUTINE NEEDED : GRAFZ.F
c       ================================================================
        real*8 s0,ks,ki,ke,kt,ktt,E
        dimension z(200,3),isymb(2),ix(40),iy(8),ig(40),zz(200,2)
        data ix,iy,ig,isymb/19*' ','TI','ME','(n','s)',65*' ','S','T'/
        data k,ns,tend/0.1,100,200/
        print *,'enter s0,ks,ki,ke,kt,ktt,E'
        read *, s0,ks,ki,ke,kt,ktt,E
        sm = 0.0001*s0
        print *,'  Ks =',ks*(+1e+9),' 1/sec',';  Ki =',ki*(+1e+9),' 1/sec'
        print *,'  Kt = ',kt*(+1e+9),' 1/sec',';  Ke = ',ke*(+1e-8),' cm**3/sec'
        print *,' CONCENTRATION [M] =',sm,'[M]',' Ktt = ',ktt*(+1e-8),'cm**3/s'
        n=0
        t=0.0
        s=0.0
        tr=0.0
        d1=0.01
        d2=d1/2.
c       ================================================================
c       USE EULER'S MODIFIED METHOD OF PREDICTOR-CORRECTOR TYPE TO SOLVE
c       THE SINGLET AND TRIPLET RATE EQUATIONS
c       ================================================================
    1   continue
c       PREDICTOR ======================================================
        s2=s+d2*(pump(t,k,sm,E)-ks*s-ke*s*(s0-s-tr))
        tr2=tr+d2*(ki*s-kt*tr-ktt*(tr**2))
c       CORRECTOR ======================================================
        t2=t+d2
        s=s+d1*(pump(t2,k,sm)-ks*s2-ke*s2*(s0-s2-tr2))
        tr=tr+d1*(ki*s2-kt*tr2-ktt*(tr2**2))
        t=t+d1
        if((n/ns)*ns.eq.n) then
         i=float(t)
         z(i,1) = t
         z(i,2) = s
         z(i,3) = tr
         zz(i,1) = t
         zz(i,2) = tr
c       PRINT TIME(ns), SINGLET VALUE, AND TRIPLET VALUE ===============
        print *,t,s,tr
        endif
        n=n+1
        if (t .lt. tend) go to 1
        do 10 i = 1,200
        if((z(i,2) -z(i+1,2)) .gt. 0.)  then
        mas = z(i,1)
        vas = z(i,2)
        go to 11
        endif
   10   continue
   11   do 12   ii = 1,200
        if((z(ii,3) - z(ii+1,3)) .gt. 0.) then
        mat = float(z(ii,1))
        vat = z(ii,3)
        write(*,15)mas,vas
   15   format( 5x,'  SINGLET PEAK    =  ',i5,'   ns',' VALUE  ',f12.4)
        write(*,16)mat,vat
   16   format( 5x,'  TRIPLET PEAK    =  ',i5,'  ns ',' VALUE  ',f12.4,/)
        go to 110
        endif
   12   continue
c       ================================================================
c       PLOT (1) TRIPLET VALUE VERSUS TIME
c            (2) SINGLET VALUE VERSUS TIME
c            (3) SINGLET AND TRIPLET VALUE VERSUS TIME
c       USE SUBROUTINE GRAFZ.F
c       ================================================================
  110   call grafz(zz,200,2,'T',1,40.,160.,0.,1.5,ix,iy,ig)
        call grafz(z,200,2,'S',1,0.,200.,0.,15.,ix,iy,ig)
        call grafz(zz,200,3,isymb,1,0.,200.,0.,15.,ix,iy,ig)
        stop
        end
c
c       ================================================================
c       THIS FUNCTION IS FOR PUMP TERM
c       ================================================================
c
        function  pump(t,k,sm,E)
        t1=20
        if(t.gt.t1) goto 1
        b=1.01*k
        g=.15
         pump=b*(1. -exp(-g*t))*(1-(10**(-E * sm)))
        return
    1   d=.05
        a = k
        pump=a*(1-(exp(-0.15*t)))*(exp(d*(t1-t)))*(1-(10**(-E * sm)))
        return
        end
```